J Mater Sci (2022) 57:21080–21103

Composites & nanocomposites

Interlaminar fracture toughness of carbon fibre composites with electrospun nanofibrous interleaves of polystyrene and cellulose nanocrystals

Konstantina Kanari[1], Michael R. Wisnom[1], Robert Harniman[2], and Stephen J. Eichhorn[1,*]

[1] Bristol Composite Institute, School of Civil, Aerospace and Mechanical Engineering, University of Bristol, Bristol BS8 1TS, UK
[2] School of Chemistry, University of Bristol, Bristol BS8 1TS, UK

Received: 11 August 2022
Accepted: 5 November 2022
Published online: 19 November 2022

ABSTRACT

Polystyrene nanofibres reinforced with cellulose nanocrystals have been produced by electrospinning. Two different orientations of the nanofibres were produced, namely aligned and random, and these nanofibrous interleaves were investigated both as-spun and after thermal treatment. Aligned nanofibres exhibited a 2500% increase in their Young's modulus compared to the randomly orientated materials, while the ultimate tensile strength increased by up to 300%. It is also demonstrated that crazing occurs in the nanofibres, which is thought to enhance the fracture properties of the materials. Interleaves of both orientations were then included in a carbon fibre-reinforced polymer laminate. The fracture toughness of the laminate was determined under both mode I and mode II testing. No increases in mode I toughness were observed. It was, however, found that the aligned interleaves increased the mode II toughness of the composite laminate (from 1.9 ± 0.3 to 2.7 ± 0.2 kJ m^{-2}). This increase is demonstrated to be due to a combination of nanofibre bridging and the formation of microcracks in the resin under applied tensile and shear load.

Introduction

Lightweight structures have been increasingly replacing metals in the aerospace and automotive industries, as their low weight can lead to reduced fuel consumption [1, 2]. The resultant reduction in carbon emissions could also have a positive outcome on the environment. Carbon fibre-reinforced polymers (CFRP) are often laminated, whereby the structure consists of plies made of a polymeric matrix and carbon fibres as a reinforcement. CFRP composites have high specific strength [1]. However, due to the nature of the materials, which for laminated systems consists of layers stacked on top of each other, the materials can suffer from delamination

Handling Editor: Dale Huber.

Address correspondence to E-mail: S.J.Eichhorn@bristol.ac.uk

https://doi.org/10.1007/s10853-022-07953-8

[3, 4]. Delamination under an applied load is the result of the material's low interlaminar fracture toughness (ILFT) [4, 5] where a crack is formed in the resin between adjacent plies [6].

Various methods have been explored for the enhancement of the ILFT of composite laminates. One approach is to delay delamination by the introduction of a resin layer between the plies, which leads to an increase in plasticity and higher fracture toughness [7]. Another common approach has been the use of micro- and nanofibrous interleaves, or veils, as plies [1, 8, 9]. These interleaves consist of nanofibres with a large aspect ratio; nanofibres with a diameter in the nanometre range (< 100 nm) are typically used. These highly affine dimensions can result in an alignment of the molecular chains in the nanofibres, which ultimately leads to enhanced structural mechanical properties (e.g. modulus, strength) [10]. The main advantages of one-dimensional nanofibres are their high surface free energy, their large length-to-diameter (aspect) ratios, and their potentially enhanced structural mechanical properties.

The incorporation of interleaves has been shown to improve the ILFT of composite laminates mostly due to two different mechanisms [8, 11]. The first is the bridging of crack zones. As the crack is formed and propagates through the resin layer containing the fibrous interleave, the nanofibres that remain intact hold the two newly formed surfaces together [1, 8]. Second, the presence of the nanofibres forces the crack to follow a longer and more complicated path through the resin, or the composite itself. This increases the required energy both for the initiation of a crack, but also for crack propagation [1, 8].

Electrospinning is an easy and efficient technique for the production of nanofibres [11–13]. These nanofibres can be incorporated in the resin layer of a composite laminate without significantly increasing their weight [14]. During electrospinning, a high voltage is applied between two electrodes. One electrode is typically the needle at the end of a syringe, and the second electrode is often an earthed or charged target on which the nanofibres are deposited [10]. The syringe typically contains a polymeric solution that is passed through the needle at a specific flow rate, usually controlled with the use of a pump [15]. As the polymeric solution exits the tip of the needle, it enters an electric field and is ejected to the grounded target [16]. As the jet travels through the electric field, the solvents evaporate rapidly, resulting in a solid continuous nanofibre [10]. When the target is a flat surface, the nanofibres are collected as a nonwoven fibrous mat. However, when the target is a rotating cylinder (or drum) then the nanofibres are deposited in an aligned orientation [17].

Ideally, the electrospun nanofibres are continuous, uniform and without surface defects or beads [18]. These characteristics will lead to uniform mechanical properties that can enhance the composite laminates' ILFT. Many parameters affect the morphology of the electrospun nanofibres; they can be divided into the solution, processing and environmental parameters [19, 20]. During electrospinning, all these parameters are in balance with each other, and their combined effects determine the nanofibres' properties [21, 22].

The incorporation of nanoparticles in nanofibres has been shown to increase their mechanical properties [23, 24]. Carbon nanotubes have been extensively used in PAN, PLA and PMMA nanofibres, while graphene has enhanced the mechanical properties of PAN, PVA and PMMA nanofibres [19]. However, a key parameter in the successful incorporation of nanoparticles in the nanofibres for this purpose is that they are well dispersed [14].

Cellulose nanocrystals (CNCs) have been used extensively in nanocomposite materials [17, 25, 26]. Cellulose is a biodegradable, natural polymer that can be used in different applications as an alternative to synthetic polymers [27]. CNCs are extracted from plant cellulose via acid hydrolysis [27–29]. They have a rodlike shape, and their dimensions vary between 3 and 50 nm in width and up to several micrometres in length [14, 27, 28]. The surface of the CNCs can be chemically modified to improve the particles' dispersion in a solution or polymer [14, 27].

In the present work, polystyrene (PS) was used to produce electrospun nanofibres containing CNCs. The CNCs were intended to alter the mechanical properties of the PS nanofibres, making them more ductile. These composite electrospun nanofibres were collected as interleaves in both random and aligned orientations. The morphology, thermal and mechanical properties of the composite nanofibres were examined, to investigate the effect of the presence of the CNCs. These nanofibrous interleaves were then incorporated into composite laminates and evaluated for mode I and mode II fracture toughness. Polystyrene is a commodity polymer that is readily processable. CNCs have been previously added in PS

fibres, but only the mechanical properties of the nanofibres were tested [17, 40, 45, 58]. To the best of our knowledge, there is no prior report on the use of electrospun PS nanofibres with incorporated CNCs to enhance the fracture properties of CFRP laminates.

Methods and materials

Materials

Polystyrene (PS) particles (molecular weight, Mw = 280 000) were purchased from Fisher Scientific (Leicestershire, UK). Cellulose nanocrystals (CNCs), sodium form, were supplied by the Process Development Center in the University of Maine (Maine, USA). N,N-Dimethylformamide (DMF) and tetrahydrofuhran (THF) of analytical grade were used as received from Fisher Scientific (Leicestershire, UK) and from Scientific Laboratory Supplies (Nottingham, UK), respectively.

Sample preparation

Solid PS particles were dissolved in a mix of DMF and THF in a ratio of 3:1; the concentration of the solutions was 20 wt% PS. CNCs were then added into this PS solution at concentrations of 0, 1, 5, 10% in relation to the added weight of PS. The solutions were initially stirred overnight at room temperature in order for the PS to be fully dissolved.

After the CNCs were added, the solutions were magnetically stirred for 1 h followed by a further hour of sonication to ensure their dispersion. All the solutions were used immediately after they were produced.

Electrospinning

An Electrospinz ES1a electrospinning rig was used for the manufacture of the PS and composite nanofibres. The dissolved polymer solution was poured into glass syringes (10 mL, blunt tip, Socorex) and transferred through PTFE tubes to metallic needles (Luer Lock, 50 mm, Supelco). The glass syringe was mounted on an electric pump (Harvard Apparatus 11 Elite Syringe Pump). The metallic needle was attached to a high voltage supply and the flat target was grounded. The temperature was centrally controlled in the lab to approximately 20 °C, and the relative humidity was monitored using a thermohydrograph. The humidity varied in the range 60–68%. The setup was in a 'parallel-to-plate' configuration for the collection of fibres of random orientation, to ensure a uniform electric field. For the collection of fibres of aligned orientation, a drum was used instead of a flat plate. The drum rotated at 2500 rpm during electrospinning.

During electrospinning, the applied voltage was 17.5 kV. The target-to-collector distance was kept constant at 15 cm. The solution's flow rate was 0.275 mL h^{-1} and the internal diameter of the needle was 0.40 mm. Thermal treatment was required to create a connected network of nanofibres. To achieve this the nanofibrous interleaves were inserted in a furnace for 2 h at 110 °C. No external pressure was used during the thermal treatment of the nanofibres in order to maintain the porosity of the networks.

Production of composite laminates

Composite laminates were produced using a layup process and then by curing in an autoclave. The prepreg that was used for the laminates was MTC 400–1 UD, purchased from SHD Composites (Lincolnshire, UK). This material is a toughened epoxy resin system with unidirectional carbon fibres designed for aerospace and motorsport applications.

Each composite laminate consisted of 24 plies of fibres of 0° orientation. In the mid-plane of the laminate, an interleave was inserted during layup. All the laminates were bagged, sealed and placed under vacuum for 24 h. Afterwards the laminates were cured in an autoclave at 100 °C for 4 h. The temperature was then increased to 180 °C and held for 2 h for post-curing. Curing occurred in an autoclave under a 6-bar pressure.

Characterisation

Fourier transform infrared (FTIR) spectroscopy (Spectrum 100 FTIR, PerkinElmer) was used to examine the nanofibres immediately after their production and three days later, to test whether there was any solvent present in the fibrous interleaves. Sixteen scans were used for accuracy, within a wavenumber range of 4000 to 650 cm^{-1}.

The internal structure of the nanofibres was mapped using atomic force microscopy (AFM). Fibrous networks were embedded in 'Epon' resin (TAAB

Labs LTD, UK) which was polymerised at 60 °C for 24 to 48 h. Following this curing, it was microtomed to reveal cross sections of the nanofibres perpendicular to their lengths. A multi-mode VIII microscope with a nanoscope V controller was used for the imaging of the cross sections. The microscope was operated in tapping mode using non-resonant PeakForce feedback control (Bruker, CA, USA).

Differential scanning calorimetry (DSC) and thermal gravimetric analysis (TGA) of the nanofibres were undertaken simultaneously with an STA 449 F3 Jupiter, High Temperature Platform 400, Netzsch system; 5 to 7 mg of each sample was tested under a nitrogen atmosphere. The analysis rate was 5 °C per minute, starting at 25 °C and ramping up to 650 °C. A single run of each sample was taken and further analysed.

Scanning electron microscopy (SEM) (Hitachi TM 3030PLus SEM and JEOL IT300 SEM) was used for the morphological characterisation of the nanofibres and networks. The fibrous networks were coated with 9 nm of silver. The samples were observed using a 15 kV acceleration voltage. SEM images were used to determine the diameters of the produced nanofibres using ImageJ image processing software. In total, 100 nanofibre diameters were measured manually, chosen randomly from the whole sample.

The mechanical properties of the fibrous interleaves were obtained using a Deben rig (Deben Microtest MT200 Tensile Tester) with a 2 N load cell. A crosshead speed of 1 mm min^{-1} was used for uniaxial tensile testing. At least 5 samples were tested for each mat. Prior to testing, the fibrous interleaves were cut into sample strips of 15 mm length and 5 mm width. The thickness of each sample was measured with a Measuring Force Digimatic Micrometer (CLM1.6"QM, Mitutoyo, Japan) at least 3 times; these thicknesses are reported for the range of samples tested in Supplementary Information. Initially the areal densities of each individual sample were measured, but it was found that due to insensitivity of these measurements that variations in these values were not detectable. Therefore, it was assumed that areal density remained constant, and a value of stress was calculated on the basis of the cross-sectional area of each individual sample. It is thought that there may well be some variation in local areal density, but this is left as a subject for future investigation. The thicknesses and widths for all samples are contained in Supplementary Information (Tables S1 and S2). Indeed, thickness of the samples is found to vary and this may be due to a variation in porosity. The samples were then carefully placed on a paper template, with epoxy glue at each end, to ensure the adhesion of the nanofibres on the template. The glued sides of the templates also acted as grips during testing. Finally, the fibrous interleaves were tested with a gauge length of 10 mm.

A double cantilever beam (DCB) test was used for the determination of the interlaminar fracture toughness in mode I (opening mode), based on ASTM D5528-13. The data reduction method that was used was the modified beam theory (MBT).The laminates were cut into rectangular samples with dimensions 140 mm (length) × 20 mm (wide) and thicknesses of 3.90 ± 0.20 mm. All samples contained a non-adhesive PTFE thin film (thickness of 0.02 mm) in the mid-plane that acted as the delamination initiator. This thin film had a 50 mm length and was placed at the end of the specimen towards the centre (Fig. 1S, Supplementary Information).

All DCB tests were performed using a Shimadzu AGS-X tensile tester fitted with 10 kN load cell. At least 3 samples were tested for each laminate type. Prior to the actual test, a pre-crack was formed in each laminate. An opening load was applied on the hinges at a crosshead rate of 1 mm min^{-1}. When a crack initiation was observed, it was allowed to propagate up to ~ 5 mm. The opening load was then stopped, and the sample was returned to its starting position at a rate of 20 mm min^{-1}.

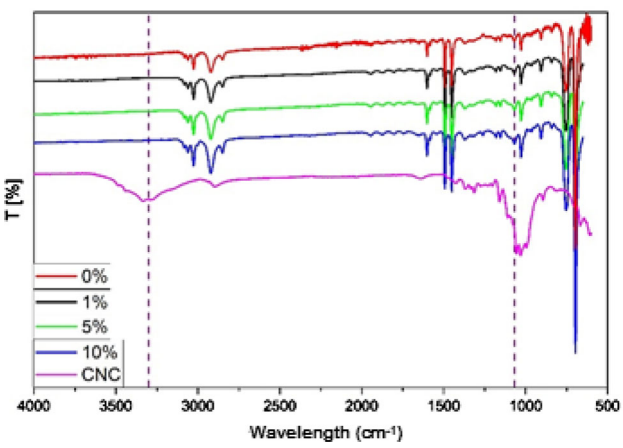

Figure 1 Typical Fourier transform infrared (FTIR) spectra for electrospun PS nanofibres, with and without CNCs, and pure CNCs. The dotted lines on the graph show the position of bands located at ~ 1260 cm^{-1} and ~ 3300 cm^{-1}.

For the test, a constant crosshead speed of 1 mm min^{-1} and a load data sampling rate of 10 Hz were used. The crosshead movement was the controlled variable, and the opening displacement, load and delamination length were all recorded with a high-resolution DSLR camera. Upon loading each specimen, the load and displacement were recorded, starting at the point at which delamination was observed. As the crack propagated through the specimen, the load and displacement were recorded for every 5 mm of delamination, starting from the tip of the pre-crack to a total length of 50 mm of delamination from the pre-crack tip.

End-notched flexure (ENF) tests were used to determine the mode II interlaminar fracture toughness G_{II} under mode II shear loading (ASTM D7905). The manufacturing of the samples was similar to those used in DCB testing, with a PTFE layer creating a crack of 50 mm in the mid-plane. Each sample had dimensions of 160 mm (length) × 20 mm (width) and a thickness of 3.90 ± 0.20 mm. For ENF testing, each sample was positioned on two cylinders at a distance of 100 mm apart, and the load was applied through a cylindrical indenter that was placed in the middle of the sample. There was no pre-crack formation prior to ENF testing (Fig. 2S, Supplementary Information).

ENF tests were performed using a Shimadzu AGS-X tensile tester fitted with 10 kN load cell. A high-resolution DSLR camera was used to record the tests in video mode. The tests were conducted at a constant crosshead speed of 0.5 mm min^{-1} and a load data acquisition rate of 10 Hz. At least 3 samples were tested for each laminate type.

For statistical purposes, t-tests were performed to determine whether data were significantly different. Analysis of datasets yielding p-values of less than 0.05 was deemed to be significantly different (95% confidence).

Results and discussion

Fourier transform infrared spectra of nanofibres

FTIR was used to examine all the electrospun fibrous interleaves. A representative spectrum of PS nanofibres without CNCs is shown in Fig. 1. There are four absorbance bands of interest: first, a band located between 650 and 770 cm^{-1}. This is attributed to -C-H out-of-plane bending vibrations due to the mono-substituted benzene in PS [30, 31]. Second, a band located between 1400 and 1600 cm^{-1} is observed, which is due to an absorbance from aromatic C–C stretching [31, 32] and -C-H bending vibrations [30, 32]. A third band in the region between 2800 and 2950 cm^{-1} indicates the presence of methylene groups [30]. Last, an absorption band between 3000 and 3100 cm^{-1} is the result of the aromatic -C-H symmetric and asymmetric stretching vibrations due to benzene ring structures in polystyrene [30–32]. Based on these data, it is concluded that the electrospun nanofibres are indeed polystyrene without the presence of any residual solvent. As the samples

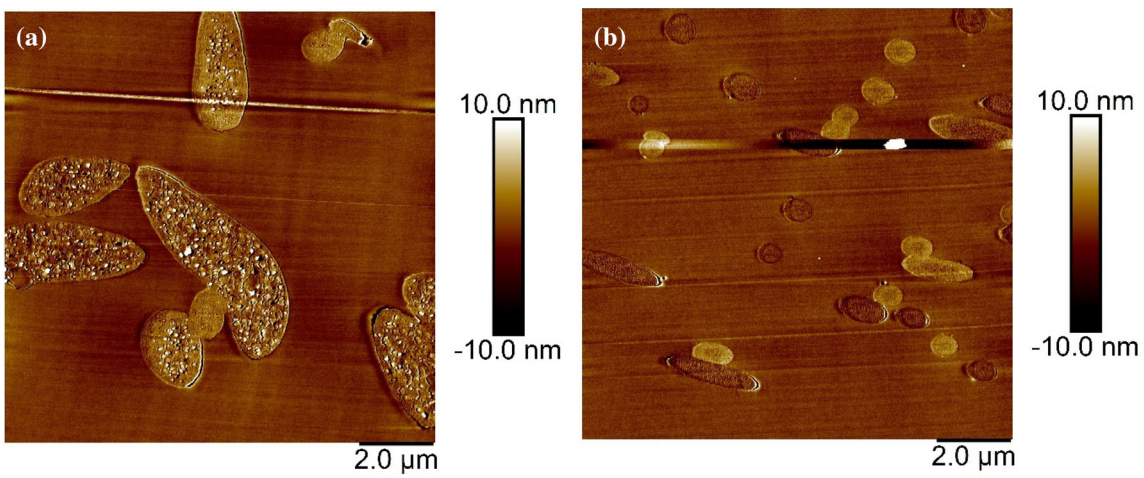

Figure 2 Typical atomic force microscope (AFM) images of electrospun PS nanofibres **a** before and **b** after annealing. The lines across the tops of the images are artefacts from the imaging.

were not degassed prior to the FTIR measurements, there is a possibility that a small quantity of solvent might still be present in the samples. The use of another analytical method would ensure that there is no residual solvents.

Figure 1 also presents FTIR spectra of PS nanofibres after the incorporation of CNCs. In these spectra, an additional absorbance band at ~ 1260 cm^{-1} was visible which became more intense with an increasing CNC concentration. This band has been assigned to -CH_2 vibrations within the cellulose structure [33, 34], indicating that the CNCs were successfully incorporated inside the PS nanofibres during electrospinning. A weak -OH group absorbance band located at ~ 3300 cm^{-1} was expected in the spectra due to the presence of CNCs. However, this band was not observed. The absence of this band is thought to be due to the low concentration of CNCs compared to the PS. For this reason, AFM measurements were taken to analyse the internal structure of the electrospun PS nanofibres in order to further locate the CNCs.

Atomic force microscopy imaging of nanofibres

AFM revealed that the as-spun nanofibres had an internal porosity with voids ~ 10 nm in depth and of widths 91 nm ± 68 nm (Fig. 2a). Additionally, similar internal structures were prominent from the plane of measurement up to ~ 10 nm. This combination created a structure of 'dips and mountains' inside the PS nanofibres. This morphology is consistent with the previous analysis reported by Pai et al. [35] and Lu and Xia [36]. They concluded that environmental humidity could induce phase separation inside the nanofibres, which leads to a porous internal structure.

After thermal treatment of the nanofibres, any internal porosity was removed (Fig. 2b). The internal structure of the nanofibres appeared homogeneous, which led to a decrease in their diameter. Pai et al. [35] also produced electrospun PS nanofibres and studied their internal structure before and after thermal treatment. An internal porosity of was initially observed for all their electrospun nanofibres. However, after thermal treatment all nanofibres condensed with diameters decreasing by up to 30%.

AFM was also used to study the incorporation of CNCs in the PS nanofibres. The study was conducted only with PS nanofibres after they had been thermally treated, as the internal porosity made it difficult to detect any CNCs. Figure 3 shows consolidated nanofibres with 5 wt% and 10 wt% CNCs. When 5 wt% CNCs was added in the nanofibres, there was only a minor change in their internal morphology. The surface roughness of a typical PS nanofibre was increased from 0.80 nm for pure PS to 0.84 nm, which is a significant difference on the scale of AFM measurements. This change indicated that there were elements on the surface of the PS nanofibres which are thought to be CNCs. Similar AFM results have been reported by Gubaa et al. [37] and Vincent et al. [38]. When the concentration of CNCs was increased to 10 wt%, two different internal structures were observed. The first was PS nanofibres that appeared completely condensed, without any difference in surface roughness. The second was PS nanofibres with a large increase in their surface roughness, of up to 1.67 nm; this was thought to be due to 'gaps' on their surfaces. These 'gaps' are thought to be the result of poor adhesion between the PS and the CNCs, where the latter have pulled out of the surrounding polymer. This indicates possible poor adhesion between the PS and CNCs resulting in the extraction of the latter by the microtome blade that cut the nanofibres. The combination of these two internal morphologies leads to the conclusion that an increased amount of CNCs results in an inhomogeneous dispersion in the PS nanofibres.

Thermal analysis of nanofibres

DSC was used to identify any change in the glass transition temperature (T_g) of the PS nanofibres with increasing CNC concentrations. The T_g of bulk PS has been reported to be ~ 100 °C [35]. Based on data from the electrospun nanofibres, the T_g for the pure PS nanofibres was ~ 111 °C, and it remained stable even when 1 wt% CNCs was added (Fig. 4). When the CNCs' concentration was increased to 5 and 10 wt%, the T_g increased to 113 °C. Typically, for constrained thin films of amorphous polymers, such as PS, a depression of the glass transition temperature occurs, although increases have also been observed. Mayes et al. [39] observed that this depression can be attributed to a localised reduction in the material's density as the result of a high number of macromolecular chain ends close to the surface of the thin film. This increase in the T_g is an indication that at a

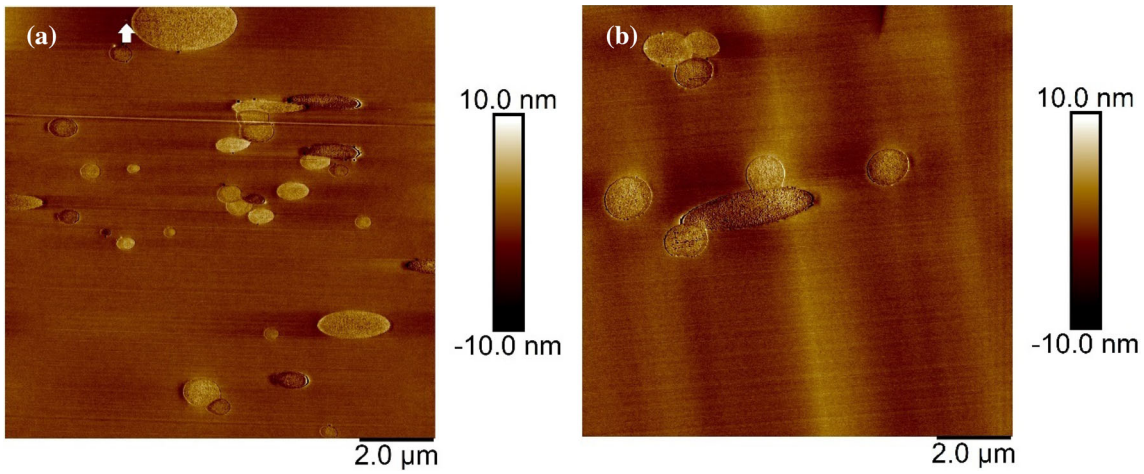

Figure 3 Typical atomic force microscope (AFM) images of PS electrospun nanofibres with **a** 5 wt% CNCs and **b** 10 wt% CNCs.

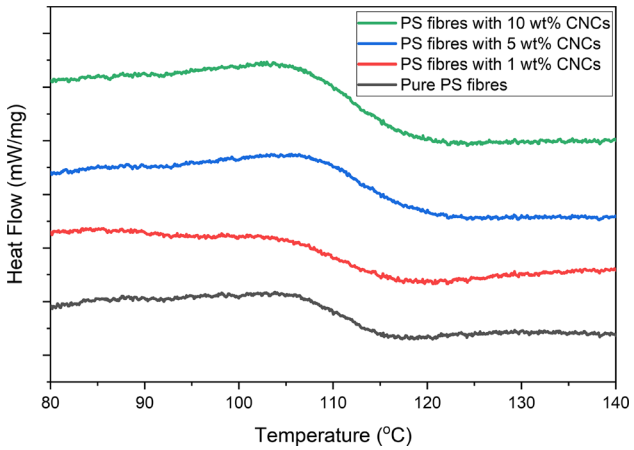

Figure 4 Typical DSC curves for the different types of fibres. From bottom to top, each interleave contains 0, 1, 5 and 10 wt% CNCs, respectively.

high concentration of CNCs they form an internal network inside the nanofibres; this network is thought to lead to an increased thermal stability of the nanofibres with a simultaneous decrease in the mobility of the molecular chains [40, 41]. Similar results have been reported by Shi et al. [42] when they examined the incorporation of CNCs in PLA nanofibres. They found that the T_g of the composite nanofibres increased by 2 °C when the concentration of the added CNCs reached 5 wt%. Bai et al. [43] studied the thermal behaviour of thin polystyrene films that were placed on top of a cross-linked PS film which was adhered on a silicon substrate. They noticed that the polystyrene thin film's T_g was affected by the cross-linking density of the polymeric substrate layer. This was attributed to the diffusion of polystyrene molecules in nanovoids that were formed in the interlayer between the cross-linked polymeric substrate and the silica substrate that was used; the diffusion led to a topological constraint of the thin polystyrene film and hence an increased T_g. Similar results were also reported by Jiang et al. [44], with the behaviour being observed on silicon substrates.

Figure 5 shows the TGA thermographs of PS nanofibres with an increase in the CNCs' concentration. The pure PS nanofibres exhibit a one-step decomposition with an onset temperature (T_{onset}) of 360 °C. When the CNCs were added, the nanofibres remained thermally stable up to ~ 246 °C. The nanofibres containing 1 wt% CNCs exhibited a single-step decomposition with a T_{onset} of ~ 331 °C.

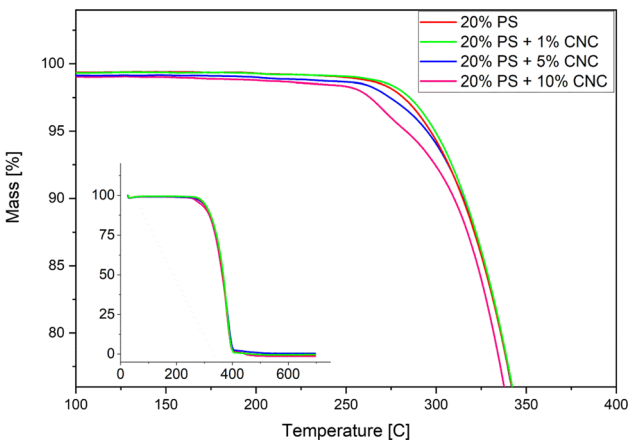

Figure 5 TGA thermographs of electrospun PS nanofibres with different concentrations of CNCs. The fibres were produced with a 20 wt% PS solution, and the different CNC concentrations were 0, 1, 5 and 10 wt%.

When the CNC concentration increased to 5 wt%, the nanofibres started to decompose with a double-step process at ~ 257 °C and a T_{onset} of ~ 332 °C. At the highest concentration of CNCs (10 wt%), the nanofibres started to decompose at an even lower temperature (~ 246 °C), with a double-step decomposition and a T_{onset} of 332 °C. This double-step decomposition is consistent with results published by Huan et al. [45] and Wang et al. [46]. Both these studies reported the effect of CNCs in electrospun nanofibres and identified a similar early decomposition of PS nanofibres as the CNCs' concentration increased. This decomposition could be attributed to the presence of sulphate groups on the surface of the CNCs, which are known to reduce the thermal stability of composites [47]. The thermal stability of CNCs has recently been critiqued and shown to depend more on the degree of surface charge than the groups themselves, and whether the sodium or acid form are used [48]. Vanderfleet et al.[48] concluded that CNCs in the sodium form are more thermally stable, compared to the acid form, and their thermal degradation is practically unchanged; any surface groups have a negligible effect to the thermal decomposition of the particles.

Nanofibre diameters

Three different variables and their effect on the nanofibre diameters were studied, namely the inclusion of increasing concentrations of CNCs, thermal treatment and the orientation of the electrospun nanofibres themselves. In all cases, the nanofibres were uniform and without beads. This meant that the concentration of the solution was high enough for entanglement of the polymer chains to produce bead-free nanofibres [49]; additionally, the electric field was strong enough to counteract the surface tension of the PS solution and result in a continuous ejection of the solution [14, 18]. The diameter of the PS nanofibres with a random orientation (Fig. 6) spun using an applied voltage of 17.5 kV, was 0.88 ± 0.22 μm. When 1 wt% CNCs was added, the nanofibres had an increased diameter of 1.76 ± 0.57 μm. Adding a second component in electrospun nanofibres is known to result in larger diameter filaments [50].

An increase in the CNC concentration to 5 wt% led to the production of nanofibres with a decreased diameter of 1.25 ± 1.02 μm. When the CNC concentration is increased, it is known that the conductivity of the solution also increases [10, 41]; this change is probably due to the presence of negatively charged sulfate half ester groups. This leads to an increased whipping instability during electrospinning and therefore nanofibres with a thinner diameter [51]. When the CNCs' concentration was further increased to 10 wt% the nanofibres had an average diameter of 1.60 ± 0.55 μm. This increase in diameter was the due to the increased viscosity of the solution in the presence of the CNCs; this increase leads to an increased quantity of solution being ejected from the needle tip due to more macromolecular entanglements of the PS [52].

The nanofibres were thermally treated to remove any internal porosity and thus increase their intrinsic mechanical properties. During the thermal treatment, there was a partial fusing at intersections between filaments due to the increased mobility of the molecular chains. Afterwards, the nanofibres were bonded together at the points of intersection by 'nodes' [53]. Typical images of the annealed PS nanofibres are reported in Fig. 7. Similar images have been reported by Xue et al. [14]. They concluded that the nanofibres were 'welded at the cross-points.' This welding or fusion leads to the creation of a connected fibrous network. Hatch et al. [54] also produced electrospun PVP nanofibres with incorporated CNCs. After a thermal treatment of the nanofibres at 200 °C for 1 h, they observed cross-linked nanofibres with fused nodes similar to the results of the present study.

After the thermal treatment, the diameters of the nanofibres were measured, the results of which are reported in Table 1. The diameters of the annealed nanofibres were found to decrease by up to 56% compared to the as-spun samples, which is attributed to their consolidation. Vadas et al. [55] studied the effect of thermal treatment on the diameter of electrospun PLA nanofibres. They documented a diameter decrease of up to 0.9 μm and suggested that 0.3 μm of this decrease was due to the evaporation of solvents, and only 0.6 μm was due to the thermal treatment itself.

Hatch et al. [54] noted that the nanofibre diameter of electrospun PVP nanofibres was affected by the addition of CNCs after annealing. They observed that the PVP nanofibres were not uniform in thickness and noted that the CNCs might not have been fully oriented during electrospinning; if these

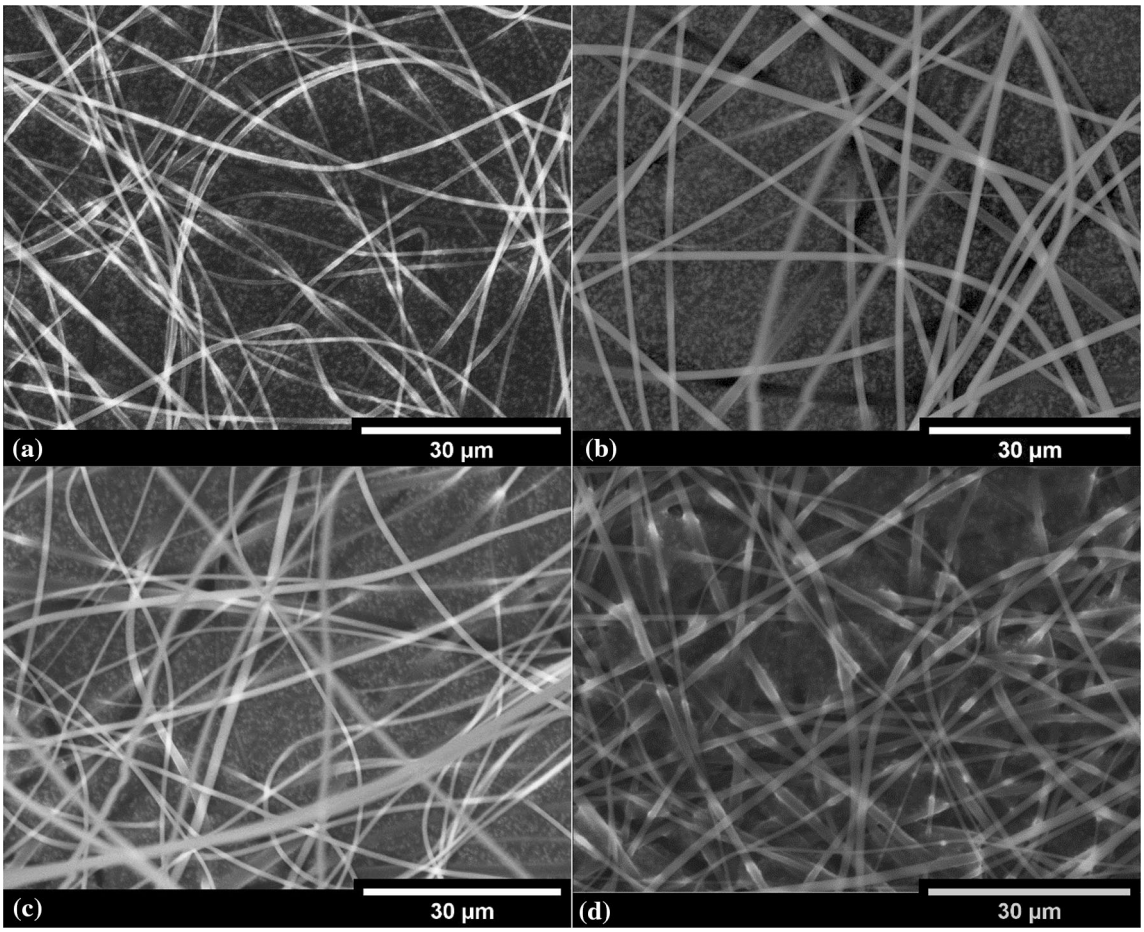

Figure 6 Typical scanning electron microscope (SEM) images of electrospun PS nanofibres with different CNC concentrations: **a** 0 wt%, **b** 1 wt%, **c** 5 wt%, **d** 10 wt%.

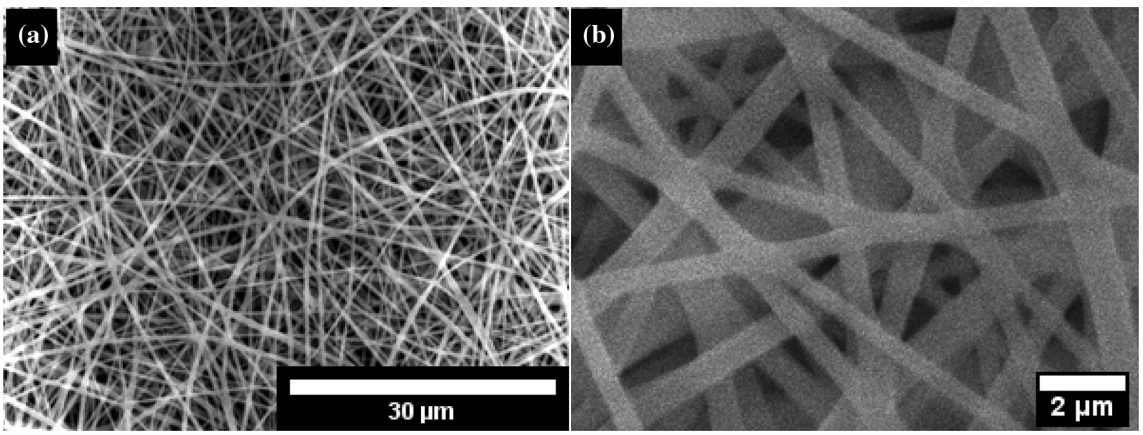

Figure 7 Typical scanning electron microscope (SEM) images of annealed nanofibres at **a** × 2000 and **b** × 10,000 magnification.

agglomerates contained non-oriented CNCs of a larger length, this could have resulted in the formation of non-uniform nanofibres. The large standard deviations that were obtained for the diameters of the as-spun nanofibres in Table 1 suggest that they appear to exhibit some of this behaviour, which suggests a similar orientation to the CNCs. Irrespective of annealing, the trend in the change in nanofibre

Table 1 Changes in the nanofibre diameter of electrospun PS nanofibres after thermal treatment and with the addition of cellulose nanocrystals (CNCs)

CNCs (%)	Random orientation			Aligned orientation		
	Status	Nanofibre size (μm)	Change	Status	Nanofibre size (μm)	Change
0%	As-spun	0.88 ± 0.22	− 17%	As-spun	0.62 ± 0.23	− 2%
	Annealed	0.73 ± 0.11		Annealed	0.61 ± 0.19	
1%	As-spun	1.76 ± 0.57	− 56%	As-spun	0.73 ± 0.34	− 4%
	Annealed	0.78 ± 0.31		Annealed	0.70 ± 0.26	
5%	As-spun	1.25 ± 1.02	− 48%	As-spun	0.63 ± 0.31	− 5%
	Annealed	0.64 ± 0.16		Annealed	0.60 ± 0.29	
10%	As-spun	1.60 ± 0.55	− 26%	As-spun	0.67 ± 0.15	− 7%
	Annealed	1.18 ± 028		Annealed	0.62 ± 0.28	

diameters when increasing the CNCs' concentration remained the same.

Figure 3S shows aligned nanofibres, both as-spun and after thermal treatment and the diameter of the fibres are reported in Table 1. The diameter of the as-spun PS nanofibres was 0.62 ± 0.23 μm. By adding 1 wt% of CNCs, the diameter was then found to be similar (0.73 ± 0.34 μm, $p > 0.05$). When 5 wt% CNCs was added, the diameter remained the same (0.63 ± 0.31 μm, $p > 0.05$). Further incorporation of 10 wt% CNCs led to no further increase (0.67 ± 0.15 μm, $p > 0.05$). The diameter of the pure PS nanofibres after the thermal treatment was 0.61 ± 0.19 μm. By adding 1 wt% CNCs, the diameter remained the same, at 0.70 ± 0.26 μm. Increasing the CNCs' concentration to 5 wt% did not significantly affect the diameter compared to the pure nanofibres (0.60 ± 0.29 μm, $p > 0.05$), and a further increase to 10 wt% led to no significant change in diameter (0.62 ± 0.28 μm, $p > 0.05$). The lack of any significant decrease in the diameter of the nanofibres indicated that the nanofibres were not porous.

A rotating drum was used for the collection of aligned PS nanofibres. However, as the nanofibres are deposited on the drum they are stretched due to the rotation, and the orientation of the molecular chains has been reported to increase because of this [17, 18, 56]. This increased orientation and stretching leads to thinner nanofibres. It is clear that the stretching of the nanofibres has an effect on the diameter of the nanofibres that overcomes any potential diameter decrease due to the incorporation of the CNCs. This could indicate an increased alignment of the CNCs inside the aligned PS nanofibres, although further investigation would be required to prove such a hypothesis.

Mechanical properties of the nanofibrous networks

Nanofibres of random orientation

Networks of pure PS nanofibres exhibited an ultimate tensile strength (UTS) of 686 ± 204 kPa and strains to failure in the range 20–50% (Fig. 8a). Young's modulus was determined to be 5.5 ± 4.6 MPa from the initial slope of the stress–strain curve (Fig. 8b). With the incorporation of 1 wt% CNCs in the nanofibres, the UTS of the networks was significantly decreased by 42% to 395 ± 64 kPa ($p < 0.05$), with strains to failure in the range 40–60%. Young's modulus was also significantly decreased by 71% to 1.5 ± 1 MPa ($p < 0.05$). When 5 wt% CNCs was included in the nanofibres, the UTS of the networks did not increase significantly (603 ± 196 kPa, $p > 0.05$), while the strains to failure decreased to values in the range 20–40%. Young's modulus decreased by 7% to 5.1 ± 2.6 ($p < 0.05$). When the concentration of CNCs increased to 10 wt% the UTS of the networks decreased to 518 ± 59 kPa ($p < 0.05$), by 25% compared to the PS nanofibres, with a strain to failure of ~ 40%. Young's modulus decreased to 1.7 ± 0.3 MPa ($p > 0.05$).

Networks (or interleaves) of electrospun nanofibres with random orientations have been more widely reported in the literature [9, 10, 15, 18, 23, 24]. These fibrous interleaves are thought to be held together by van der Waal's forces between the filaments [57]. The UTS obtained for the networks of pure PS nanofibres is higher than the previously reported value of 0.15 MPa [45] by up to 360%. However, with the incorporation of the CNCs there was either no difference, or a decrease in the mechanical properties of the nanofibrous networks, compared to the pure PS

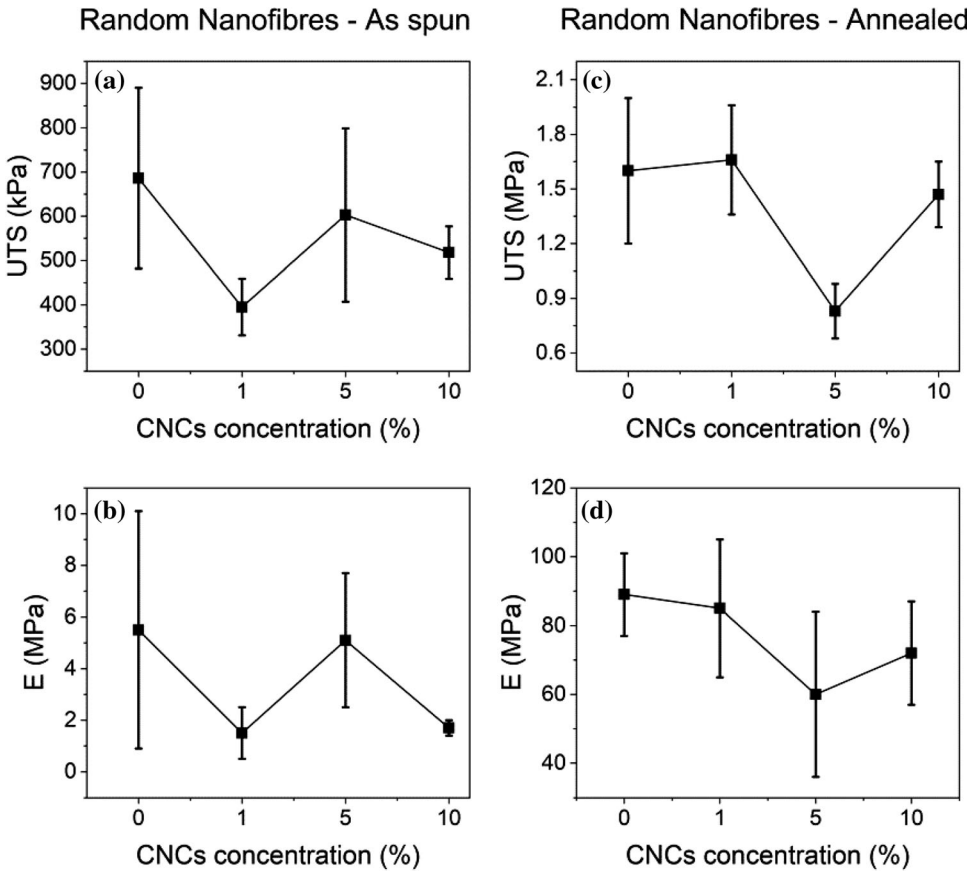

Figure 8 Summary of the calculated Young's modulus (E) and UTS values for random nanofibres, tested as-spun (**a**, **b**) and (**c**, **d**) after annealing.

nanofibres. It is thought that this is the result of the inherent incompatibility of the hydrophilic CNCs and the hydrophobic PS polymer. When the CNCs are added in the PS solution, they tend to agglomerate, resulting in nanofibres with CNC-rich and CNC-poor areas. Agglomerates have been reported to increase the mechanical properties of the PS nanofibrous networks [41, 45]. However, it is more likely that they act as defects and crack initiators resulting in nanofibre failure and a low UTS of the whole network [58].

Huan et al. [45] observed that the incorporation of CNCs in PS nanofibres led to a 170% increase in the interleaves' measured UTS, compared to interleaves of pure PS nanofibres. On the other hand, Kalantari et al. [58] concluded that the addition of CNCs without surface modifications did not enhance the mechanical properties of electrospun PS nanofibrous networks. When Huan et al. [56] studied the inclusion of CNCs in PLA nanofibres, another hydrophobic polymer, the results were similar to what is presented here; the aggregation of CNCs at high concentration led to a significant decrease in the networks' mechanical properties.

Pai et al. [59] concluded that the main parameter affecting the modulus of a fibrous network is the orientation of the nanofibres. Similar conclusions were drawn by Tan et al. [60], when they studied the mechanical properties of PCL nanofibrous networks. During the electrospinning of random nanofibres, there is typically a variation in the areal density of the deposited network [61]. During tensile testing of random nanofibres, it is primarily those filaments that are aligned to the axis of the applied deformation that carry the load until they undergo local failure. Testing continues with nanofibres being aligned to the applied load and fracturing locally until catastrophic failure of the network occurs [61, 62]. Therefore, depending on the areal density and the random orientation of nanofibres, the results of tensile testing can exhibit significant variations [12, 13].

Farukh et al. [63] studied electrospun polypropylene nanofibrous networks and observed them rotating towards the axes of the applied load before failure. This behaviour continued until the samples

failed. Furthermore, Farukh et al. [64] used computational modelling to study this behaviour. They concluded that after the samples reached 50% strain the number of nanofibres that could carry any external load was significantly reduced. This change in the nanofibre orientation is shown in Fig. 4S (Supplementary information) showing an interleave before and after testing; proportionally more nanofibres are observed to have oriented towards the tensile direction after deformation.

With regard to the interleaves of random orientation after annealing, the UTS of annealed networks of pure PS nanofibres was initially found to be 1.60 ± 0.40 MPa (Fig. 8c). Young's modulus was found to be 89 ± 12 MPa (Fig. 8d). When 1 wt% CNCs was added to the nanofibres the UTS of the interleave was not found to increase (1.66 ± 0.3 MPa, $p > 0.05$), while Young's modulus remained the same (85 ± 20 MPa, $p > 0.05$). An increase in the CNC concentration to 5 wt% significantly decreased both the UTS by 47% to 0.83 ± 0.15 MPa ($p < 0.05$) and Young's modulus by 33% to 60 ± 24 MPa ($p < 0.05$). When 10 wt% of CNCs were added to the nanofibres a UTS of 1.47 ± 0.18 MPa ($p > 0.05$) and a Young's modulus of 72 ± 15 MPa ($p > 0.05$) were obtained for the interleaves. All samples catastrophically failed at strains in the range 2.5–3.6%, without a significant difference to the pure PS nanofibrous interleaves.

The consolidation of the nanofibres and the formation of surface nodes led to an increase in both the UTS and Young's modulus of all the nanofibrous interleaves, compared to their as-spun counterparts. Young's modulus increased by up to 10 times for the annealed interleaves, consistent with previously published results [35, 60, 65]. The surface nodes were of particular interest in the mechanical testing of annealed fibrous interleaves. These nodes acted as 'anchors' between the nanofibres, that allowed the applied load to be carried by the majority of the filaments and not only the ones already oriented towards the axis of the applied load. Nevertheless, as the nanofibres were fused together the re-orientation of them due to the applied load was not possible and the interleave failed at lower strains.

Pai et al.[35] observed an increase in Young's modulus of electrospun PS nanofibres from 1.24 to 3.57 GPa due to annealing. Similarly, their UTS increased from 17 to 49 MPa. Farukh et al. [66] studied electrospun PP nanofibrous networks both experimentally and computationally. They observed that the nodes increased the stiffness of the fibrous interleaves, but there was negligible deformation before failure. Similar results were presented by Chavoshnejad et al. [67, 68] when they calculated the effect of nodes in PMMA interleaves.

SEM was used to identify the failure mechanisms of the annealed samples. Figure 9 shows a typical SEM image of an annealed interleave of nanofibres with random orientation before and after tensile testing. Three main failure mechanisms are identified in the fibrous interleaves: necking, shear banding and crazing. Specifically crazing is observed as a dark vertical deformation perpendicular to the axis of the applied load [69]. Figure 5S (Supplementary Information) shows the fibrils that were formed at the point of failure in the annealed nanofibres due to crazing. It is worth noting that all three mechanisms were observed in both pure PS nanofibres and those containing CNCs. However, no crazing was observed after testing of the as-spun random nanofibres. The internal porosity of the nanofibres is thought to suppress any crazing in the nanofibres, as has previously been observed [70].

Nanofibres of aligned orientation

As-spun fibrous interleaves of aligned orientation were mechanically tested, but only as pure PS nanofibres and with 5 wt% of CNCs (Fig. 10a). The pure PS nanofibres exhibited a UTS of 2.89 ± 0.73 MPa, which remained the same when the CNCs were added (3.56 ± 0.97 MPa, $p > 0.05$). Young's modulus of the pure PS nanofibres was 148 ± 38 MPa, a value that significantly increased by 93% to 285 ± 84 MPa ($p < 0.05$) when CNCs were added. The strain at break was not determined as the samples exhibited a steplike gradual failure.

Regarding the annealed nanofibres, PS nanofibres were measured both with and without the presence of CNCs, the former with 1, 5 and 10 wt% concentrations (Fig. 10b). Young's modulus of the different interleaves continuously increased with the addition of CNCs. The pure PS nanofibres had a Young's modulus of 285 ± 90 MPa, a value that remained the same when 1 wt% CNCs was added in the nanofibres (281 ± 37 MPa, $p > 0.05$). When 5 wt% CNCs was added in the nanofibres, Young's modulus significantly increased by 59% to 454 ± 132 MPa ($p < 0.05$). The addition of 10 wt% CNCs increased this to

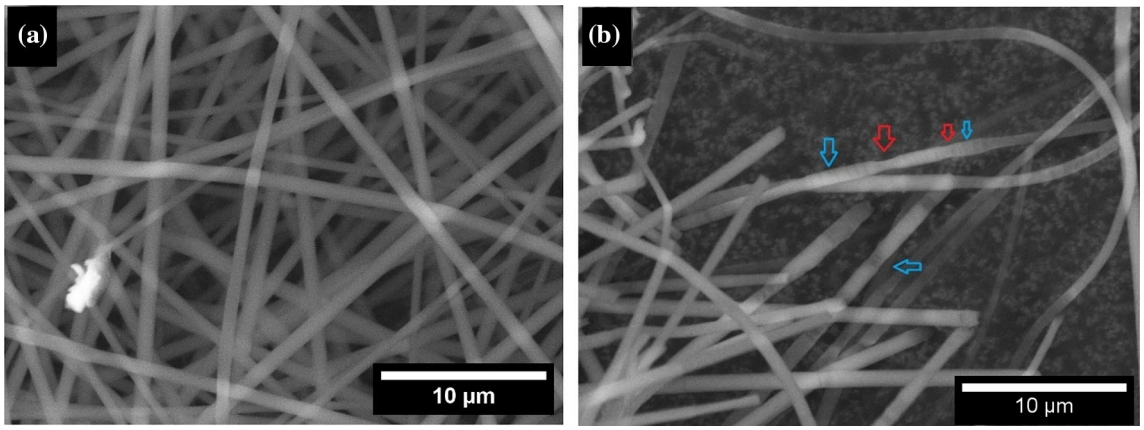

Figure 9 Typical scanning electron microscope (SEM) images of random PS nanofibres after they have been thermally treated; **a** nanofibres before tensile testing; **b** an image of the nanofibres after tensile testing. The red arrows identify the location of necking in the nanofibres, and the blue arrows show where crazing is thought to have occurred.

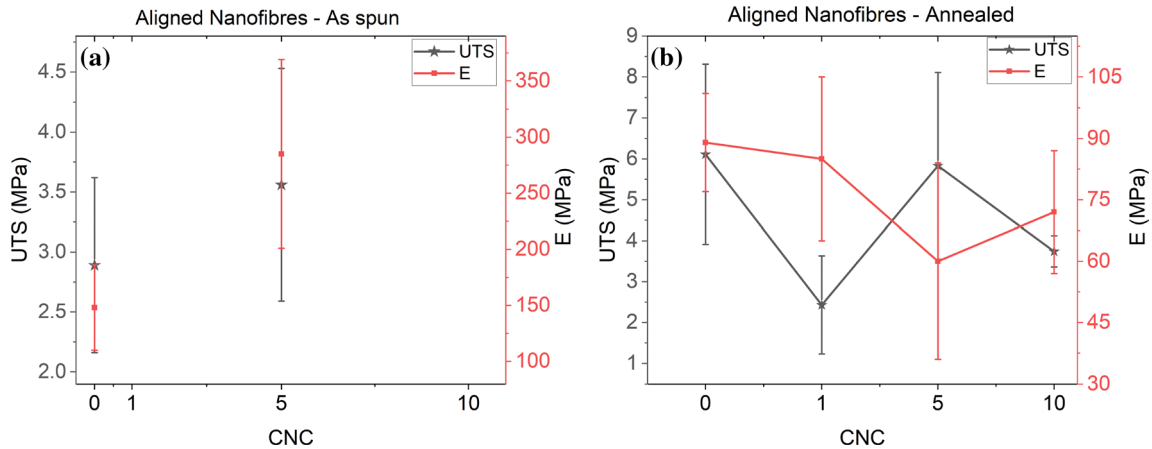

Figure 10 Summary of the calculated Young's modulus (E) and UTS values for aligned nanofibres, tested **a** as-spun and **b** after annealing.

790 ± 194 MPa, a significant increase of 177% compared to the pure PS nanofibres ($p < 0.05$).

The UTS of the aligned annealed nanofibres was 6.11 ± 2.20 MPa, which significantly decreased by 60% with the addition of 1 wt% CNCs to 2.43 ± 1.20 ($p < 0.05$). By increasing the CNCs to 5 wt%, the nanofibres' UTS did not change (5.83 ± 2.28 MPa; $p > 0.05$). Finally, by adding 10 wt% CNCs in the nanofibres the UTS was 3.74 ± 0.38 MPa ($p > 0.05$). The large standard deviation associated with these values was attributed to a large number of samples tested, each of which contained fibres of random orientation; it has been previously shown in the literature that the UTS of the samples is largely affected by the different orientations of the nanofibres in each sample [61, 63, 64, 66].

All the mechanical properties of fibrous interleaves with aligned orientation were significantly increased compared to fibrous interleaves with random nanofibres. Young's modulus of pure PS as-spun nanofibres increased by more than 2500% compared to the random nanofibres ($p < 0.05$), while the UTS increased by more than 30% ($p < 0.05$). Moreover, Young's modulus of aligned annealed PS nanofibres increased by 220% and the UTS by 282% ($p < 0.05$). These results are similar to the data presented by Thomas et al. [71]; they managed to increase Young's modulus of PCL nanofibres by 900% just by alignment of the nanofibres. Similarly, Huang et al. [72] obtained a 400% increase in Young's modulus for aligned nanofibres compared to a random orientation. These increases are thought to be the result of a combination of effects. First, when the nanofibres are deposited on a rotating collector, they are further stretched due to the rotation. Therefore, the molecular chains are thought to orient towards the axis of

the nanofibres, which enables them to withstand higher stresses before catastrophic failure [17, 56]. Moreover, the number of nanofibres that carry the load at any given moment during tensile testing is increased [41, 73]. Last, due to the increased alignment of the macromolecular chains in the nanofibres, it can be argued that the incorporated CNCs will also be aligned; this alignment could enhance the nanofibres' modulus due to the inherently stiff nature of the CNCs [17]. Lee et al. [74] studied how the mechanical properties of electrospun PVA nanofibres were affected by the orientation of the deposited nanofibres. They concluded that the UTS and Young's modulus of the fibrous networks were increased when the degree of the nanofibre alignment was increased. Similar results were presented by Huan et al.[56] for PLA nanofibres. They also noted that an increase of more than 5 wt% added CNCs was detrimental to mechanical properties.

Mode I fracture toughness of a composite laminate

Mode I testing of composite laminates was performed in order to calculate the fracture toughness at initiation ($G_{Ic,ini}$) and during propagation ($G_{Ic,\ prop}$) before and after an insertion of an electrospun interleave comprising PS and CNCs. The average areal weight of each interleave was approximately 3.6 g m^{-2}, while the average nanofibre diameter was 0.66 ± 0.29 μm for the aligned nanofibres and 1.11 ± 0.50 μm for the random nanofibres. $G_{Ic,ini}$ was calculated at the onset of the nonlinear region of the measurements, to avoid any influence of the value due to carbon fibre bridging [75, 76]; hence, the calculated values are thought to be conservative [77].

Nine different types of interleaves were tested, and at least 3 samples for each type of laminate. First, a composite laminate without an interleave was tested as a baseline. Then, 4 types of interleaves with nanofibres of random orientation; the nanofibres had an increasing amount of CNCs at 0, 1, 5 and 10 wt%. Last, 4 interleaves were tested, with nanofibres of aligned orientation; the CNC concentrations in the nanofibres were again 0, 1, 5 and 10 wt%. In all the laminates containing fibrous interleaves, variation was observed between the samples of the same laminate. This variation was attributed to differences in areal thickness and nanofibre orientation of the interleaves [78].

Random nanofibres

$G_{Ic,ini}$ for the baseline sample (without any interleave) was 163.9 ± 19.4 J m^{-2} (see Fig. 11), a value comparable to the work of Hojo et al. [79] and Beckermann et al. [75]. $G_{Ic,\ prop}$ was 404.3 ± 118.0 J m^{-2}, but it was clear that this value increased continuously during the testing. This increase was attributed to fibre bridging of the carbon filaments in the unidirectional samples. Nanofibre bridging was observed (Fig. 6S, Supplementary Information); visible carbon fibres at the crack tip of the opening and at the fracture surface after testing were observed. Carbon fibre bridging in unidirectional laminates has often been reported in the literature [3, 79, 80].

The calculated G_I values for laminates with random nanofibre interleaves are also shown in Fig. 11. For the laminate with random pure PS nanofibres, $G_{Ic,ini}$ was found to significantly decrease to a value of 107.7 ± 5.9 J m^{-2} ($p < 0.05$, compared to the baseline sample). When the nanofibres contained 1 wt% CNCs, $G_{Ic,ini}$ was 102.2 ± 9.7 J m^{-2} ($p > 0.05$, compared to the pure random sample). When the CNCs' concentration increased to 5 wt%, $G_{Ic,ini}$ remained unchanged at 109.7 ± 12.6 J m^{-2} ($p > 0.05$). The

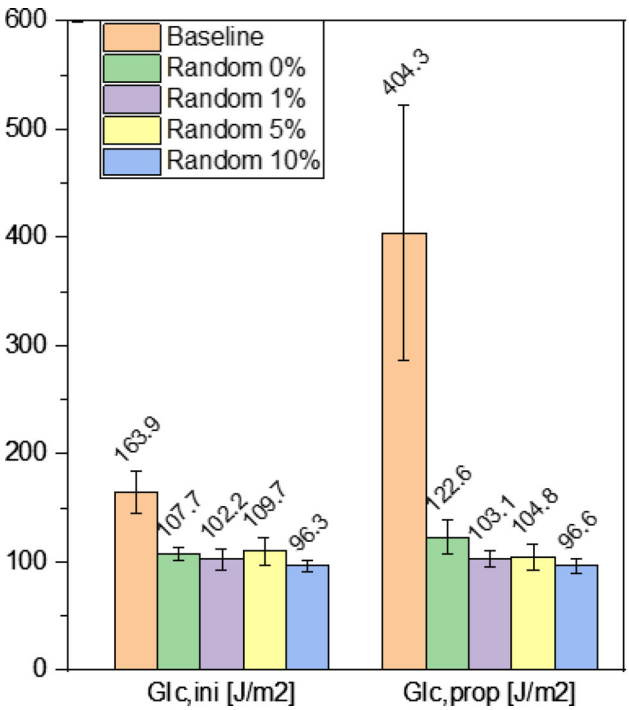

Figure 11 Fracture toughness values (mode I) at initiation ($G_{Ic,ini}$) and propagation ($G_{Ic,prop}$) for the baseline laminate and laminates containing interleaves of random nanofibres.

$G_{Ic,\ prop}$ values for the different laminates were calculated. $G_{Ic,\ prop}$ for the pure PS interleave was 122.6 ± 16.1 J m^{-2}. With nanofibres containing 1 wt% CNCs, $G_{Ic,prop}$ decreased by 16% to 103.1 ± 7.9 J m^{-2} ($p < 0.05$). Nanofibres containing 5 wt% CNCs led to a 15% decrease of $G_{Ic,prop}$ to 104.8 ± 11.9 J m^{-2} ($p < 0.05$), compared to samples with an interleave with pure PS nanofibres. Nanofibres with 10 wt% CNCs caused a further decrease of the $G_{Ic,prop}$ to 96.5 ± 6.87 J m^{-2} ($p < 0.05$).

The main observation from all data is that there is a decrease in G_{Ic} values when a fibrous interleave is incorporated into the laminate. This was mainly attributed to the suppression of carbon fibre bridging during testing [80]. Furthermore, the SEM images of the laminate surface after testing show no evidence of bridging or necking by the nanofibres (Fig. 7S, Supplementary Information). The nanofibres completely peeled off the resin, as it can be seen from the imprints that have been left behind. Additionally, the nanofibres show a clear rupture at their points of failure rather than ductile necking. That leads to the conclusion that the decrease of G_{Ic} was the result of debonding of the nanofibres from the matrix [75, 80, 81]. Similarly, Daelemans et al. [80] observed a decrease of $G_{Ic,ini}$ from 538 J m^{-2} to 322 J m^{-2} with the presence of a PA6 interleave (3 g m^{-2}) and a decrease of the $G_{Ic,prop}$ from 829 to 491 J m^{-2}. Beckermann et al.[75] and Zhang et al. [81] attributed nanofibre debonding to poor adhesion to the epoxy resin. One cause of the debonding could have been trapped air or moisture that was released from the nanofibres during the curing of the laminates. Air or moisture could act as a 'defect' in the resin causing premature failure [82], although we have no evidence to confirm this.

As the CNCs tend to aggregate inside the nanofibres, they became more brittle, and this is also thought to also occur inside the laminate. The combination of the brittleness of the nanofibres with the CNCs' aggregation acting as areas of stress concentration possibly led to failure at lower loads, as has been seen before [38]. This could result in premature failure of the nanofibres containing CNCs compared to the pure PS nanofibres [17, 46]. Wang et al.[46] observed that an addition of 3 wt% CNCs in PEI nanofibres, however, resulted in a 20% increase of $G_{Ic,ini}$. But when 5 wt% of CNCs were added a 28% decrease in $G_{Ic,ini}$ occurred, which may have been due to the effect of increased aggregation.

Aligned nanofibres

Figure 12 shows the calculated G_{Ic} values for composite laminates with fibrous interleaves of aligned orientation. The laminate with a fibrous interleave of pure PS had a G_{Ic} of 155.3 ± 14.2 J m^{-2}. When 1 wt% CNCs was added to the nanofibres, G_{Ic} remained the same at 154.6 ± 15.7 J m^{-2} ($p > 0.05$). With the addition of 5 wt% CNCs in the nanofibres, the G_{Ic} decreased by 20% to 124.5 ± 17.1 J m^{-2} ($p < 0.05$). A 32% decrease was observed for the interleave with 10 wt% CNCs to 117.8 ± 7.7 J m^{-2} ($p < 0.05$). The $G_{Ic,prop}$ value for the laminate with pure PS nanofibres was 141.1 ± 8.0 J m^{-2}. 1 wt% CNCs in the nanofibres led to a 6% increase in $G_{Ic,prop}$ to 150.3 ± 10.1 J m^{-2} ($p < 0.05$). When 5 wt% CNCs was incorporated in the nanofibres, $G_{Ic,prop}$ decreased to 123.4 ± 11.3 J m^{-2} ($p < 0.05$). Last, the addition of 10 wt% CNCs decreased the $G_{Ic,prop}$ value to 120.3 ± 2.9 J m^{-2} ($p < 0.05$).

Both G_{Ic} and $G_{Ic,prop}$ values were lower than the baseline laminate values, which is attributed to the poor adhesion of the aligned nanofibres to the resin. Bovicelli et al. [83] observed a 3.2% decrease in $G_{Ic,ini}$ when a PCL interleave was incorporated in a

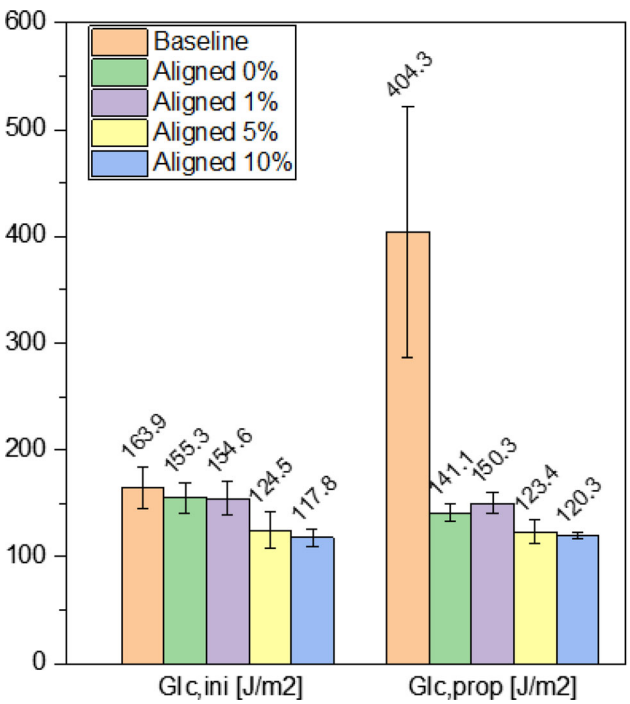

Figure 12 Fracture toughness (mode I) values at initiation ($G_{Ic,ini}$) and propagation ($G_{Ic,prop}$) for the baseline laminate and laminates containing interleaves of aligned nanofibres.

composite laminate and a 3.4% decrease when the interleave was made of Nylon 6,6. Beckermann et al. [75] and Kageyama et al. [84] studied the effect of interleaves in composite laminates and they both reported higher $G_{Ic,ini}$ values compared to $G_{Ic,prop}$. The values for aligned interleaves were higher than values for interleaves of random nanofibres. This is most likely the result of the different mechanical properties of the aligned nanofibres compared to the random interleave. Kalantari et al. [17] suggested that the decreased diameter of the aligned nanofibres might lead to an increased orientation of the macromolecular chains inside the nanofibres. This could lead to enhanced mechanical properties which in turn could lead to an improved fracture toughness.

Mode II testing

Mode II testing of the composite laminates was used to measure the fracture toughness at initiation under shear forces (G_{IIc}) for each laminate. Nine different types of interleave were tested; a composite laminate without an interleave was used as a baseline. Four types of interleaves with nanofibres of random and aligned orientations were tested. The nanofibres of both orientations included CNCs with concentrations of 0, 1, 5 and 10 wt%. Similar to mode I testing, there were variations observed between the samples of the same laminate. These variations were the result of differences in areal thickness and nanofibre orientation, as has been previously observed [78]. For that reason, at least 3 samples were tested for each laminate.

Random nanofibres

G_{IIc} for the baseline sample was calculated as 1.9 ± 0.3 kJ m^{-2}. When an interleave of pure PS was added in the laminate, G_{IIc} was found to remain the same (1.6 ± 0.1 kJ m^{-2}, $p > 0.05$). When 1 wt% CNCs was added in the nanofibres G_{IIc} dropped by 29% to 1.2 ± 0.4 kJ m^{-2} ($p < 0.05$). 5 wt% CNCs in the nanofibres led to a similar G_{IIc} of 1.6 ± 0.3 kJ m^{-2} ($p > 0.05$), while 10 wt% CNCs decreased the G_{IIc} by 21% to 1.3 ± 0.1 kJ m^{-2} ($p < 0.05$). All these values are summarised in Fig. 13a.

The incorporation of pure PS nanofibres did not significantly change the G_{IIc} of the laminate, which could be indicative of the lack of nanofibre bridging during testing [85]. Any change of the G_{IIc} could be a result of the interleaves' aerial weight [75]. In contrast, an increase in the amount of CNCs incorporated into the nanofibres led to a significant decrease in G_{IIc}.

According to Zhang et al. [81], the incorporation of CNCs into nanofibres without any surface treatment can result in a decrease in G_{IIc}.

In Fig. 14, the SEM image of the surface of a composite laminate with an interleave after mode II testing has been magnified. It was clear that the resin had penetrated through the random nanofibres, as both nanofibres and indents of nanofibres can be seen at different heights from the surface. This surface morphology is also indicative of a crack propagation through the random network of nanofibres. Some nanofibres are present that also show partial debonding from the resin. Furthermore, typical matrix debris and hackle marks are also evident after mode II testing. Hackle marks are typical of failure under shear stresses in composite laminate testing [85, 86]. The crack path during mode II testing is also observed to move from inside the resin layer to the interface between the resin and the carbon fibres. Such observations are consistent with the published literature [7].

Aligned nanofibres

The G_{IIc} for the laminate with pure PS nanofibres was calculated as 2.6 ± 0.2 kJ m^{-2}, a significant increase of 38% compared to the baseline composite ($p < 0.05$). When 1 wt% CNCs was added in the nanofibres, the G_{IIc} was found to be unchanged at 2.6 ± 0.1 kJ m^{-2} ($p > 0.05$). With a further increase in the CNC concentration to 5 wt% the laminates, G_{IIc} of the laminate did not change (2.6 ± 0.2 kJ m^{-2}, $p > 0.05$). Finally, by further increasing the CNC content to 10 wt% the G_{IIc} remained stable at 2.7 ± 0.2 kJ m^{-2} ($p > 0.05$). The results of all the calculations are summarised in Fig. 13b.

The incorporation of an interleave with aligned nanofibres required a higher load to fail, leading to a higher value of G_{IIc}. This was the result of nanofibre bridging in mode II testing that enhances the toughness of the material under shear load. Daelemans et al. [86] used PA 6.9 aligned nanofibres as interleaves in composite laminates. They found that G_{IIc} increased by 50% due to nanofibrous bridging of microcracks. Nevertheless, the addition of any amount of CNCs did not alter the properties of the

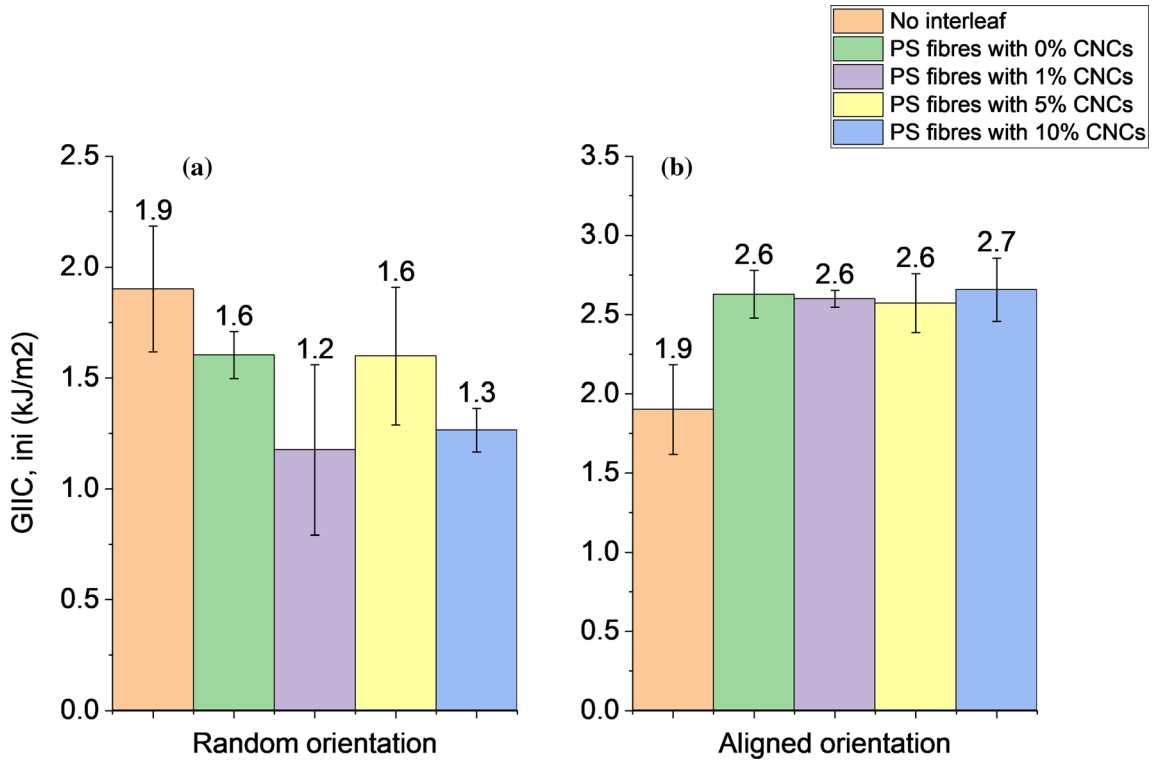

Figure 13 **a** Fracture toughness values for mode II (G_{IIc}) testing for the baseline laminate and laminates containing interleaves of **a** random nanofibres and **b** of aligned nanofibres, with different concentrations of cellulose nanocrystals (CNCs).

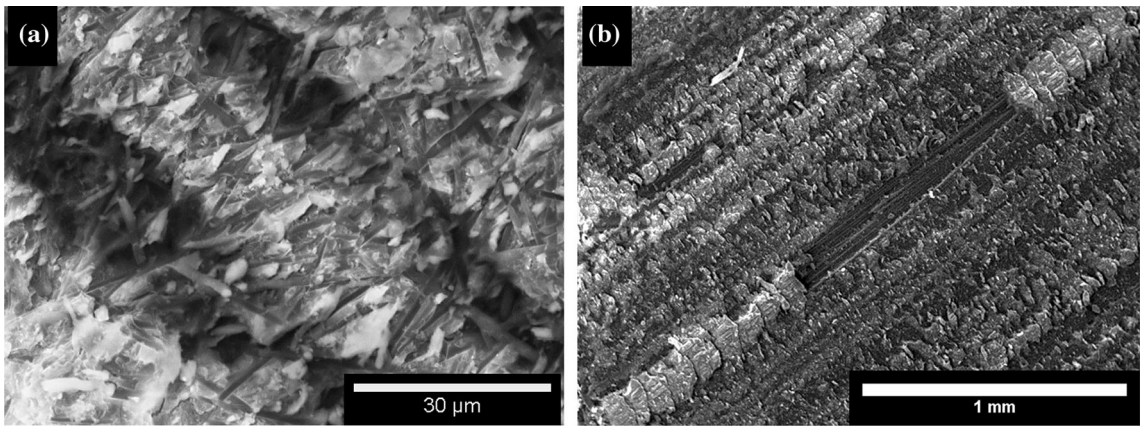

Figure 14 Scanning electron microscope (SEM) images of a composite laminate containing an interleave of random nanofibres after mode II testing.

composite laminates when the nanofibres were aligned. Li et al. [87] studied the incorporation of different concentrations of multi-wall carbon nanotubes in electrospun PSF nanofibres as interleaves. It was reported that G_{IIc} increased with the addition of these nanofibrous interleaves in the laminates.

Discussion

The addition of CNCs in electrospun PS nanofibres did not significantly affect the mechanical properties of the nanofibres. This is thought to be due to the incompatibility between the CNCs and the PS polymer. Even though crazing as a toughening mechanism was observed in the nanofibres, the CNCs did not significantly increase the degree of crazing.

Nanoinclusions in nanofibres and amorphous polymers have previously resulted in the initiation of crazes [88]. Instead, the poor dispersion of CNCs inside the nanofibres is thought to cause stress concentrations which leads to the decrease in the nanofibres' UTS. The agglomeration and lack of full alignment of CNCs in electrospun nanofibres has been previously highlighted as a reason as to why the theoretical mechanical properties are not obtained [89]. The addition of active groups on the surface of the CNCs could potentially lead to a better adhesion of the CNCs and the PS nanofibres and hence the induction of crazing at a larger scale, making the nanofibres more ductile and thereby leading to enhanced fracture toughness of the laminated composites.

Two techniques that enhanced the nanofibres' mechanical properties were the thermal treatment of the interleaves and the alignment of the nanofibres. Thermal treatment led to the consolidation of the porous PS nanofibres and the creation of fused nodes at the points of contacts. The consolidation of porous PS nanofibres has been shown to increase their mechanical properties [35]. The nodes led to a uniform distribution of the applied load on the fibrous sample and thereby an increased UTS and Young's modulus compared to the as-spun nanofibres. The alignment of the nanofibres had a twofold effect: First, the production process of the nanofibres decreased their diameter, and potentially, the macromolecular chains inside the nanofibres were then more orientated to the axis of the nanofibres. Second, the alignment of the nanofibres led to a more uniform distribution of the applied load on the whole sample, leading to an enhanced Young's modulus and UTS. The largest enhancement of the electrospun nanofibres was observed in samples that were both thermally treated and aligned.

The main mechanisms that could be used for the enhancement of the mechanical properties of CFRP laminates with interleaves are bridging of nanofibres and crack deflection. It has been suggested that plastic deformation of ductile materials is necessary for high fracture toughness values during testing of composite laminates [90]. However, since the epoxy matrix of most CFRP laminates is brittle, a ductile material would be beneficial for the increase in ILFT in composite laminates. Hence, it is unsurprising that most published research [8, 90] has been based on electrospun interleaves of ductile polymers, such as PAN and PCL.

PS is an inherently brittle material and the incorporation of CNCs did not enhance its ductility. Therefore, any increase in ILFT in the tested composite laminates were mostly due to the alignment of nanofibres. With respect to the thermal treatment of the nanofibres, all the interleaves that were used were as-spun. In mode I, both random and aligned interleaves led to a decrease in the laminate's G_I. This was attributed the different nature of epoxy matrix and the polystyrene nanofibres, which led to low adhesion between the two materials. Compatibility between the matrix and the interleave is crucial in the toughening of composite laminates [90]. During testing of the laminate, the low adhesion of the nanofibres led to the nanofibres being pulled out of the matrix. They also did not form any stable crack bridges during this process. Furthermore, due to the brittle nature of the PS nanofibres, the crack was not deflected around the nanofibres in the epoxy but instead caused their failure at low loads. Even though alignment of the nanofibres influenced the G_I, these values were still lower than the values obtained from a composite laminate without an interleave, a result of the lack of carbon fibre bridging due to the insertion of the interleave. Surface modification of the PS nanofibres would be advisable for increased adhesion between the two materials that could potentially lead to nanofibre bridging.

Regarding mode II testing, the incorporation of aligned nanofibres increased the CFRP laminate's G_{IIc}, something that was not observed when random nanofibres were used. Even though the toughening mechanisms behind mode II fracture are not yet fully understood [90], ILFT depends not only on nanofibre bridging, but also on a combination of tensile and shear microcrack growth. Furthermore, the addition of nanofibres of high tensile strength can lead to an increased mode II ILFT [90] that could explain why the inclusion of aligned nanofibres led to an increase in G_{II} compared to a laminate without an interleave or one comprising random nanofibres.

In both mode I and mode II testing, the random nanofibres decreased the fracture toughness of the baseline laminate (laminate without any interleave). This result has already been attributed mainly to the low adhesion between the PS nanofibres and the epoxy matrix. However, the low porosity of the interleave due to the high coverage of the nanofibres

could also have restricted the infusion of the resin inside the interleave. In a recent review paper, Vallack and Sampson [90] state that fibrous veils made of micron-sized fibres increases the fracture toughness of laminates, whereas nanofibrous veils have little effect, both in mode I and mode II testing. The improved resin infusion when micron-sized fibres are used could also result in resin-rich areas inside the interleave increasing the toughness of the laminate. This conclusion is in agreement with our results, where nanofibres of random orientation reduced the fracture toughness of the laminates. In the future PS micron-sized fibres of random orientation could be used to further investigate this. Nonetheless, we suggest that it is the alignment of the nanofibres of the interleave that seems to dominate the interleaves' toughening effect.

Conclusions

Polystyrene nanofibres were produced using an electrospinning technique. The nanofibres contained varying amounts of CNCs, and they had two different orientations: random and aligned. These nanofibres were morphologically analysed and mechanically tested, and subsequently added as interleaves in the mid-plane of composite laminates. The laminates were studied in mode I and mode II testing. It was found that annealing of the fibrous networks was necessary to bond the nanofibres to each other, but to also remove porosity of the nanofibres. Both these led to an increase in the overall mechanical properties of the networks.

Both Young's modulus and ultimate tensile strength (UTS) of the fibres were negatively affected by the inclusion of CNCs when the samples were as-spun. It was thought to be the result of the difference between the hydrophobic PS and the hydrophilic CNCs that led to the nanofibres failing at low applied loads. When the nanofibres were aligned, their mechanical properties increased compared to their random counterparts: Young's modulus and UTS increased by approximately 2600% and 320%, respectively. Similarly, when annealed pure PS nanofibres were tested, Young's modulus and UTS increased by 220% and 282%, respectively. These increases suggested that the orientation of the nanofibres plays a major role in the mechanical properties of the networks and inherently the nanofibres within those networks. This could be due to the production of the aligned nanofibres that leads to further stretching of the nanofibres after electrospinning. That could increase the orientation of the macromolecular chains inside the nanofibres and in turn enhance their mechanical properties under axial load.

Composite laminates were successfully tested with nanofibrous interleaves in their mid-plane to study the effect of the nanofibre orientation on the fracture toughness of the laminates. When the interleave was made of random nanofibres, the nanofibres decreased the fracture toughness of the material. That was attributed to the nanofibres inhibiting carbon fibre bridging during testing. Furthermore, the aggregation of CNCs inside most likely acted as stress concentrations leading to failure at lower loads.

When the interleaves comprised aligned nanofibres, the laminates exhibited similar behaviour to mode I testing with the random nanofibres. In mode II testing, the fracture toughness of the laminates was increased by 35% compared to a laminate with no interleave. The alignment of the nanofibres seemed to be optimal for testing in shear loading, and the enhanced mechanical properties of the aligned nanofibres might have contributed to this. No significant difference was observed amongst the different CNC concentrations that were used.

Acknowledgements

The authors would like to thank the Engineering and Physical Sciences Research Council for the funding of a Centre for Doctoral Training grant to support K.K. (EP/L016028/1).

Funding

This study was funded by the Engineering and Physical Sciences Research Council (EPSRC) (grant number EP/L016028/1).

Declarations

Conflict of interest The authors declare that they have no conflict of interest.

Supplementary Information: The online version contains supplementary material available at https://doi.org/10.1007/s10853-022-07953-8.

References

[1] Di BY, Joshi SC (2020) A review of methods for improving interlaminar interfaces and fracture toughness of laminated composites. Mater Today Commun 22:100830. https://doi.org/10.1016/j.mtcomm.2019.100830

[2] Shakil UA, Shukur |, Hassan BA, et al (2020) Mechanical properties of electrospun nanofiber reinforced/interleaved epoxy matrix composites—a review. Polym Compos 41:2288–2315. https://doi.org/10.1002/pc.25539

[3] Pozegic TR, King SG, Fotouhi M et al (2019) Delivering interlaminar reinforcement in composites through electrospun nanofibres. Adv Manuf Polym Comp Sci 5:155–171. https://doi.org/10.1080/20550340.2019.1665226

[4] Shrivastava R, Singh KK (2020) Interlaminar fracture toughness characterization of laminated composites: a review. Polym Rev 60:542–593. https://doi.org/10.1080/15583724.2019.1677708

[5] Shakil UA, Hassan SBA, Yahya MY, Nauman S (2020) Mechanical properties of electrospun nanofiber reinforced/interleaved epoxy matrix composites—a review. Polym Compos 41:2288–2315. https://doi.org/10.1002/pc.25539

[6] Riccio A (2008) Delamination in the context of composite structural design. Delamination behaviour of composites: a volume in Woodhead Publishing Series in Composites Science and Engineering, pp 28–64. https://doi.org/10.1533/9781845694821.1.28

[7] Singh S, Partridge IK (1995) Mixed-mode fracture in an interleaved carbon-nanofibre/epoxy composite. Compos Sci Technol 55:319–327. https://doi.org/10.1016/0266-3538(95)00062-3

[8] Palazzetti R, Zucchelli A (2017) Electrospun nanofibers as reinforcement for composite laminates materials—a review. Compos Struct 182:711–727. https://doi.org/10.1016/j.compstruct.2017.09.021

[9] Zucchelli A, Focarete ML, Gualandi C, Ramakrishna S (2011) Electrospun nanofibers for enhancing structural performance of composite materials. Polym Adv Technol 22:339–349. https://doi.org/10.1002/pat.1837

[10] Andrady AL (2008) Science and technology of polymer nanofibers, 1st ed. Wiley-Blackwell

[11] Raju IS, O'Brien TK (2008) Fracture mechanics concepts, stress fields, strain energy release rates, delamination initiation and growth criteria. In: Delamination Behaviour of Composites: A volume in Woodhead Publishing Series in Composites Science and Engineering. Elsevier Ltd, pp 3–27

[12] Hou X, Acar M, Silberschmidt VV (2011) Non-uniformity of deformation in low-density thermally point bonded nonwoven material: Effect of microstructure. J Mater Sci 46:307–315. https://doi.org/10.1007/s10853-010-4800-1

[13] Rawal A, Priyadarshi A, Lomov SV et al (2010) Tensile behaviour of thermally bonded nonwoven structures: Model description. J Mater Sci 45:2274–2284. https://doi.org/10.1007/s10853-009-4152-x

[14] Xue J, Wu T, Dai Y, Xia Y (2019) Electrospinning and electrospun nanofibers: methods, materials, and applications. Chem Rev 119:5298–5415. https://doi.org/10.1021/acs.chemrev.8b00593

[15] Almetwally AA, El-Sakhawy M, Elshakankery MH, Kasem MH (2017) Technology of nano-fibers: production techniques and properties—critical review. Journal of the Textile Association 78:5–14

[16] Mishra RK, Mishra P, Verma K et al (2018) Electrospinning production of nanofibrous membranes. Environ Chem Lett 1–34. https://doi.org/10.1007/s10311-018-00838-w

[17] Kalantari M, McDermott M, Ayranci C, Boluk Y (2020) Fabrication of oriented electrospun cellulose nanocrystals–polystyrene composite fibers on a rotating drum. J Appl Polym Sci 48942:1–14. https://doi.org/10.1002/app.48942

[18] Afshari M (2017) Electrospun nanofibers. Woodhead Publishing

[19] Zhang C-L, Yu S-H (2014) Nanoparticles meet electrospinning: recent advances and future prospects. Chem Soc Rev 43:4423. https://doi.org/10.1039/c3cs60426h

[20] Baji A, Mai YW, Wong SC et al (2010) !!Electrospinning of polymer nanofibers: Effects on oriented morphology, structures and tensile properties. Compos Sci Technol

70:703–718. https://doi.org/10.1016/j.compscitech.2010.01.010

[21] Gugulothu D, Barhoum A, Afzal SM, et al (2019) Structural multifunctional nanofibers and their emerging applications

[22] Gugulothu D, Barhoum A, Nerella R, et al (2019) Fabrication of nanofibers: electrospinning and non-electrospinning techniques. In: Handbook of nanofibers. Springer Nature Switzerland, pp 45–77

[23] Wang G, Yu D, Kelkar AD, Zhang L (2017) Electrospun nanofiber: Emerging reinforcing filler in polymer matrix composite materials. Prog Polym Sci 75:73–107

[24] Mohammadzadehmoghadam S, Dong Y, Jeffery Davies I (2015) Recent progress in electrospun nanofibers: Reinforcement effect and mechanical performance. J Polym Sci, Part B: Polym Phys 53:1171–1212. https://doi.org/10.1002/polb.23762

[25] Grishkewich N, Mohammed N, Tang J, Tam KC (2017) Recent advances in the application of cellulose nanocrystals. Curr Opin Colloid Interface Sci 29:32–45. https://doi.org/10.1016/j.cocis.2017.01.005

[26] Yadav C, Saini A, Maji PK (2018) Cellulose nanofibres as biomaterial for nano-reinforcement of poly[styrene-(ethylene-co-butylene)-styrene] triblock copolymer. Cellulose 25:449–461. https://doi.org/10.1007/s10570-017-1567-4

[27] George J, Sabapathi SN (2015) Cellulose nanocrystals: synthesis, functional properties, and applications. Nanotechnol Sci Appl 8:45–54. https://doi.org/10.2147/NSA.S64386

[28] Redondo A, Jang D, Korley LTJ et al (2020) Electrospinning of cellulose nanocrystal-reinforced polyurethane fibrous mats. Polymers (Basel) 12:1021. https://doi.org/10.3390/polym12051021

[29] Foster EJ, Moon RJ, Agarwal UP et al (2018) Current characterization methods for cellulose nanomaterials. Chem Soc Rev 47:2511–3006. https://doi.org/10.1039/C6CS00895J

[30] Fang J, Xuan Y, Li Q (2010) Preparation of polystyrene spheres in different particle sizes and assembly of the PS colloidal crystals. SCIENCE CHINA Technol Sci 53:3088–3093. https://doi.org/10.1007/s11431-010-4110-5

[31] Nitanan T, Opanasopit P, Akkaramongkolporn P et al (2012) Effects of processing parameters on morphology of electrospun polystyrene nanofibers. Korean J Chem Eng 29:173–181. https://doi.org/10.1007/s11814-011-0167-5

[32] MacOssay J, Ybarra AVR, Arjamend FA et al (2012) Electrospun polystyrene-multiwalled carbon nanotubes: imaging, thermal and spectroscopic characterization. Des Monomers Polym 15:197–205. https://doi.org/10.1163/156855511X615065

[33] Kumar A, Singh Negi Y, Choudhary V, Kant Bhardwaj N (2020) Characterization of Cellulose Nanocrystals Produced by Acid-Hydrolysis from Sugarcane Bagasse as Agro-Waste. J Mater Phys Chem 2:1–8. https://doi.org/10.12691/jmpc-2-1-1

[34] Garside P, Wyeth P (2004) Identification of cellulosic nanofibres by ftir spectroscopy: thread and single nanofibre analysis by attenuated total reflectance. Stud Conserv 48:269–275. https://doi.org/10.1179/sic.2003.48.4.269

[35] Pai CL, Boyce MC, Rutledge GC (2009) Morphology of porous and wrinkled fibers of polystyrene electrospun from dimethylformamide. Macromolecules 42:2102–2114. https://doi.org/10.1021/ma802529h

[36] Lu P, Xia Y (2013) Maneuvering the internal porosity and surface morphology of electrospun polystyrene yarns by controlling the solvent and relative humidity. Langmuir 29:7070–7078. https://doi.org/10.1021/la400747y

[37] Gubała D, Harniman R, Eloi JC et al (2020) Multiscale characterisation of single synthetic nanofibres: Surface morphology and nanomechanical properties. J Colloid Interface Sci 571:398–411. https://doi.org/10.1016/j.jcis.2020.03.051

[38] Vincent S, Prado R, Kuzmina O et al (2018) Regenerated cellulose and willow lignin blends as potential renewable precursors for carbon fibers. ACS Sustain Chem Eng 6:5903–5910. https://doi.org/10.1021/acssuschemeng.7b03200

[39] Mayes AM (1994) Glass transition of amorphous polymer surfaces. Macromolecules 27:3114–3115

[40] Huan S, Bai L, Liu G, Han G (2015) Supporting information for electrospun nanofibrous composites of polystyrene and cellulose nanocrystals: manufacture and characterization Preparation of spinning solution with different conditions

[41] Gong X, Kalantari M, Aslanzadeh S, Boluk Y (2020) Interfacial interactions and electrospinning of cellulose nanocrystals dispersions in polymer solutions: a review. J Dispersion Sci Technol. https://doi.org/10.1080/01932691.2020.1847137

[42] Shi Q, Zhou C, Yue Y et al (2012) Mechanical properties and in vitro degradation of electrospun bio-nanocomposite mats from PLA and cellulose nanocrystals. Carbohyd Polym 90:301–308. https://doi.org/10.1016/j.carbpol.2012.05.042

[43] Bai L, Luo P, Yang X et al (2022) Enhanced glass transition temperature of thin polystyrene films having an underneath cross-linked layer. ACS Macro Lett 11:210–216. https://doi.org/10.1021/acsmacrolett.1c00611

[44] Jiang N, Cheung J, Guo Y et al (2018) Stability of adsorbed polystyrene nanolayers on silicon substrates. Macromol Chem Phys 219. https://doi.org/10.1002/macp.201700326

[45] Huan S, Bai L, Liu G et al (2015) Electrospun nanofibrous composites of polystyrene and cellulose nanocrystals: manufacture and characterization. RSC Adv 5:50756–50766. https://doi.org/10.1039/C5RA06117B

[46] Wang J, Pozegic TR, Xu Z et al (2019) Cellulose nanocrystal-polyetherimide hybrid nanofibrous interleaves for enhanced interlaminar fracture toughness of carbon nanofibre/epoxy composites. Compos Sci Technol 182:107744. https://doi.org/10.1016/j.compscitech.2019.107744

[47] Börjesson M, Sahlin K, Bernin D, Westman G (2018) Increased thermal stability of nanocellulose composites by functionalization of the sulfate groups on cellulose nanocrystals with azetidinium ions. J Appl Polym Sci 135:45963. https://doi.org/10.1002/app.45963

[48] Vanderfleet OM, Reid MS, Bras J et al (2019) Insight into thermal stability of cellulose nanocrystals from new hydrolysis methods with acid blends. Cellulose 26:507–528. https://doi.org/10.1007/s10570-018-2175-7

[49] Huan S, Liu G, Han G et al (2015) Effect of experimental parameters on morphological, mechanical and hydrophobic properties of electrospun polystyrene fibers. Materials 8:2718–2734. https://doi.org/10.3390/ma8052718

[50] Tjong SChin, Mai YW (2010) Physical properties and applications of polymer nanocomposites. Woodhead Pub.

[51] Hohman MM, Shin M, Rutledge G, Brenner MP (2001) Electrospinning and electrically forced jets. II Appl Phys Fluids 13:2221–2236. https://doi.org/10.1063/1.1384013

[52] Zhang Q, Li Q, young tm et al (2019) a novel method for fabricating an electrospun poly(vinyl alcohol)/cellulose nanocrystals composite nanofibrous filter with low air resistance for high-efficiency filtration of particulate matter. ACS Sustainable Chemistry and Engineering. https://doi.org/10.1021/acssuschemeng.9b00605

[53] Rittenhouse J, Wijeratne R, Orler EB et al (2019) Effect of areal density and fiber orientation on the deformation of thermomechanical bonds in a nonwoven fabric. Polym Eng Sci 59:311–322. https://doi.org/10.1002/pen.24907

[54] Hatch KM, Hlavatá J, Paulett K et al (2019) Nanocrystalline cellulose / polyvinylpyrrolidone fibrous composites prepared by electrospinning and thermal crosslinking. Int J Polym Sci. https://doi.org/10.1155/2019/7103936

[55] Vadas D, Nagy ZK, Csontos I et al (2020) Effects of thermal annealing and solvent-induced crystallization on the structure and properties of poly(lactic acid) micronanofibres produced by high-speed electrospinning. J Therm Anal Calorim 142:581–594. https://doi.org/10.1007/s10973-019-09191-8

[56] Huan S, Liu G, Cheng W et al (2018) Electrospun poly(lactic acid)-based fibrous nanocomposite reinforced by cellulose nanocrystals: impact of fiber uniaxial alignment on microstructure and mechanical properties. Biomacromol 19:1037–1046. https://doi.org/10.1021/acs.biomac.8b00023

[57] Lingaiah S, Shivakumar K (2013) Electrospun high temperature polyimide nanopaper. Eur Polymer J 49:2101–2108. https://doi.org/10.1016/j.eurpolymj.2013.04.030

[58] Kalantari M, Du R, Ayranci C, Boluk Y (2018) Effects of interfacial interactions and interpenetrating brushes on the electrospinning of cellulose nanocrystals-polystyrene fibers. J Colloid Interface Sci 528:419–430. https://doi.org/10.1016/j.jcis.2018.04.089

[59] Pai CL, Boyce MC, Rutledge GC (2011) On the importance of fiber curvature to the elastic moduli of electrospun nonwoven fiber meshes. Polymer 52:6126–6133. https://doi.org/10.1016/j.polymer.2011.10.055

[60] Tan EPS, Ng SY, Lim CT (2005) Tensile testing of a single ultrafine polymeric fiber. Biomaterials 26:1453–1456. https://doi.org/10.1016/j.biomaterials.2004.05.021

[61] Yilmaz KB, Sabuncuoglu B, Yildirim B, Silberschmidt VV (2020) A brief review on the mechanical behavior of nonwoven fabrics. J Eng Fibers Fabr 15:155892502097019. https://doi.org/10.1177/1558925020970197

[62] Jubera R, Ridruejo A, González C, Llorca J (2014) Mechanical behavior and deformation micromechanisms of polypropylene nonwoven fabrics as a function of temperature and strain rate. Mech Mater 74:14–25. https://doi.org/10.1016/j.mechmat.2014.03.007

[63] Farukh F, Demirci E, Sabuncuoglu B et al (2014) Numerical analysis of progressive damage in nonwoven fibrous networks under tension. Int J Solids Struct 51:1670–1685. https://doi.org/10.1016/j.ijsolstr.2014.01.015

[64] Farukh F, Demirci E, Sabuncuoglu B et al (2014) Mechanical behaviour of nonwovens: analysis of effect of manufacturing parameters with parametric computational model. Comput Mater Sci 94:8–16. https://doi.org/10.1016/j.commatsci.2013.12.040

[65] Tan EPS, Lim CT (2006) Effects of annealing on the structural and mechanical properties of electrospun polymeric nanofibres. Nanotechnology 17:2649–2654. https://doi.org/10.1088/0957-4484/17/10/034

[66] Farukh F, Demirci E, Sabuncuoglu B et al (2012) Numerical modelling of damage initiation in low-density thermally bonded nonwovens. Comput Mater Sci 64:112–115. https://doi.org/10.1016/j.commatsci.2012.05.038

[67] Chavoshnejad P, Alsmairat O, Ke C, Razavi MJ (2021) Effect of interfiber bonding on the rupture of electrospun fibrous mats. J Phys D Appl Phys 54. https://doi.org/10.1088/1361-6463/abba95

[68] Chavoshnejad P, Razavi MJ (2020) Effect of the interfiber bonding on the mechanical behavior of electrospun fibrous

mats. Sci Rep 10. https://doi.org/10.1038/s41598-020-64735-5

[69] Kramer EJ (1983) Microscopic and molecular fundamentals of crazing advances in polymer science. In: Kausch HH (ed) Crazing in polymers. Springer-Verlag, Berlin, pp 1–53

[70] Kim GM, Lach R, Michler GH, Chang YW (2005) The mechanical deformation process of electrospun polymer nanocomposite fibers. Macromol Rapid Commun 26:728–733. https://doi.org/10.1002/marc.200500023

[71] Thomas V, Jose MV, Chowdhury S et al (2006) Mechano-morphological studies of aligned nanofibrous scaffolds of polycaprolactone fabricated by electrospinning. J Biomater Sci Polym Ed 17:969–984. https://doi.org/10.1163/156856206778366022

[72] Huang C, Chen S, Reneker DH et al (2006) High-strength mats from electrospun poly(p-phenylene biphenyltetracarboximide) nanofibers. Adv Mater 18:668–671. https://doi.org/10.1002/adma.200501806

[73] Dong H, Strawhecker KE, Snyder JF et al (2012) Cellulose nanocrystals as a reinforcing material for electrospun poly(methyl methacrylate) fibers: Formation, properties and nanomechanical characterization. Carbohyd Polym 87:2488–2495. https://doi.org/10.1016/j.carbpol.2011.11.015

[74] Lee J, Deng Y (2012) Increased mechanical properties of aligned and isotropic electrospun PVA nanofiber webs by cellulose nanowhisker reinforcement. Macromol Res 20:76–83. https://doi.org/10.1007/s13233-012-0008-3

[75] Beckermann GW, Pickering KL (2015) Mode I and Mode II interlaminar fracture toughness of composite laminates interleaved with electrospun nanofibre veils. Compos A Appl Sci Manuf 72:11–21. https://doi.org/10.1016/j.compositesa.2015.01.028

[76] Daelemans L, Van Der Heijden S, De Baere I et al (2015) Bisphenol A based polyester binder as an effective interlaminar toughener. Compos B Eng 80:145–153. https://doi.org/10.1016/j.compositesb.2015.05.044

[77] ASTM D5528–01 (2014) Standard test method for mode I interlaminar fracture toughness of unidirectional fiber-reinforced polymer matrix composites. Am Stand Test Methods 03:1–12. https://doi.org/10.1520/D5528-13.2

[78] Beylergil B, Tanoğlu M, Aktaş E (2017) Enhancement of interlaminar fracture toughness of carbon fiber–epoxy composites using polyamide-6,6 electrospun nanofibers. J Appl Polym Sci 134:45244. https://doi.org/10.1002/app.45244

[79] Hojo M, Ando T, Tanaka M et al (2006) Modes I and II interlaminar fracture toughness and fatigue delamination of CF/epoxy laminates with self-same epoxy interleaf. Int J Fatigue 28:1154–1165. https://doi.org/10.1016/j.ijfatigue.2006.02.004

[80] Daelemans L, van der Heijden S, De Baere I et al (2015) Nanofibre bridging as a toughening mechanism in carbon/epoxy composite laminates interleaved with electrospun polyamide nanofibrous veils. Compos Sci Technol 117:244–256. https://doi.org/10.1016/j.compscitech.2015.06.021

[81] Zhang Z, Fu K, Li Y (2021) Improved interlaminar fracture toughness of carbon fiber/epoxy composites with a multi-scale cellulose fiber interlayer. Comp Commun 27:100898. https://doi.org/10.1016/j.coco.2021.100898

[82] Masoodi R, El-Hajjar RF, Pillai KM, Sabo R (2012) Mechanical characterization of cellulose nanofiber and bio-based epoxy composite. Mater Des 36:570–576. https://doi.org/10.1016/j.matdes.2011.11.042

[83] Bovicelli F, Saghafi H, Brugo TM et al (2014) On Consideration the Mode I Fracture Response of CFRP Composite Interleaved by Composite Nanofibers. Procedia Materials Science 3:1316–1321. https://doi.org/10.1016/j.mspro.2014.06.213

[84] Kageyama K, Kimpara I, Ohsawa I, et al (1995) Mode I and Mode II delamination growth of interlayer toughened carbon/epoxy (T800H/3900–2) composite system. In: ASTM Special Technical Publication. ASTM International, pp 19–37

[85] Daelemans L, Van Der Heijden S, De Baere I et al (2016) Damage-resistant composites using electrospun nanofibers: a multiscale analysis of the toughening mechanisms. ACS Appl Mater Interfaces 8:11806–11818. https://doi.org/10.1021/acsami.6b02247

[86] Daelemans L, van der Heijden S, De Baere I et al (2016) Using aligned nanofibres for identifying the toughening micromechanisms in nanofibre interleaved laminates. Compos Sci Technol 124:17–26. https://doi.org/10.1016/j.compscitech.2015.11.021

[87] Li G, Li P, Zhang C et al (2008) Inhomogeneous toughening of carbon fiber/epoxy composite using electrospun polysulfone nanofibrous membranes by in situ phase separation. Compos Sci Technol 68:987–994. https://doi.org/10.1016/j.compscitech.2007.07.010

[88] Arjmandi R, Hassan A, Eichhorn SJ et al (2015) Enhanced ductility and tensile properties of hybrid montmorillonite/cellulose nanowhiskers reinforced polylactic acid nanocomposites. J Mater Sci 50:3118–3130. https://doi.org/10.1007/s10853-015-8873-8

[89] Wanasekara ND, Santos RPO, Douch C et al (2016) Orientation of cellulose nanocrystals in electrospun polymer nanofibres. J Mater Sci 51:218–227. https://doi.org/10.1007/s10853-015-9409-y

[90] Vallack N, Sampson WW (2022) Materials systems for interleave toughening in polymer composites. J Mater Sci 57:6129–6156. https://doi.org/10.1007/s10853-022-06988-1